

# Chemical Evolution of Dwarf Irregular and Blue Compact Galaxies

J. Yin<sup>1,2</sup>, F. Matteucci<sup>2,3</sup>, G. Vladilo<sup>3</sup>

<sup>1</sup> Key Laboratory for Research in Galaxies and Cosmology, Shanghai Astronomical Observatory, CAS, 80 Nandan Road, Shanghai, 200030, China. e-mail: jyin@shao.ac.cn

<sup>2</sup> Department of Physics, Astronomy Division, Trieste University, Via G.B. Tiepolo 11, 34131 Trieste, Italy. e-mail: yin--matteucci@oats.inaf.it

<sup>3</sup> Osservatorio Astronomico di Trieste, INAF, Via G.B. Tiepolo 11, 34131 Trieste, Italy. e-mail: vladilo@oats.inaf.it

Preprint online version: November 11, 2021

## ABSTRACT

**Aims.** Dwarf irregular and blue compact galaxies are very interesting objects since they are relatively simple and unevolved. We aim at deriving the formation and chemical evolution history of late-type dwarf galaxies, and compare it with DLA systems.

**Methods.** We present new models for the chemical evolution of these galaxies by assuming different regimes of star formation (bursting and continuous) and different kinds of galactic winds (normal and metal-enhanced). The dark-to-baryonic mass ratio is assumed to be 10 in these models. The chemical evolution model follows in detail the evolution of He, C, N, O, S, Si and Fe. We have collected the most recent data on these galaxies and compared with our model results. We have also collected data for Damped-Lyman  $\alpha$ -systems.

**Results.** Our results show that in order to reproduce all the properties of these galaxies, including the spread in the chemical abundances, the star formation should have proceeded in bursts and the number of bursts should be not larger than 10 in each galaxy, and that metal-enhanced galactic winds are required. A metal-enhanced wind efficiency increasing with galactic mass can by itself reproduce the observed mass-metallicity relation although also an increasing efficiency of star formation and/or number and/or duration of bursts can equally well reproduce such a relation.

**Conclusions.** Metal enhanced winds together with an increasing amount of star formation with galactic mass are required to explain most of the properties of these galaxies. Normal galactic winds, where all the gas is lost at the same rate, do not reproduce the features of these galaxies. On the other hand, a global increase of the amount of star formation (increasing efficiency and/or number of bursts and/or burst duration) with galactic mass is able by itself to reproduce the mass-metallicity relation even without winds, but without metal-enhanced winds is not able to explain many other constraints. We suggest that these galaxies should have suffered a different number of bursts varying from 2 to 10 and that the efficiency of metal-enhanced winds should have been not too high ( $\lambda_{mw} \sim 1$ ). We predict for these galaxies present time Type Ia SN rates from 0.00084 and 0.0023 per century. Finally, by comparing the abundance patterns of Damped Lyman- $\alpha$  objects with our models we conclude that they are very likely the progenitors of the present day dwarf irregulars.

**Key words.** Galaxies: evolution - Galaxies: abundance - Galaxies: dwarf - Galaxies: irregular

## 1. Introduction

Galaxy formation and evolution is one of the fundamental problems in astrophysics. According to hierarchical clustering models, larger galactic structures build up and grow through the accretion of dwarf galaxies which are the first structures to collapse and form stars (White & Frenk 1991; Kauffmann et al. 1993). These building-block galaxies are too faint and small to be studied at high redshifts, while a class of nearby metal-deficient dwarf galaxies offer a much better chance of understanding it (Thuan 2008).

Dwarf galaxies, defined arbitrarily as galaxies having an absolute magnitude fainter than  $M_B \sim -18$  mag, are the most numerous (about 80% – 90%) galaxies in the nearby universe (Mateo 1998; Grebel 2001; Karachentsev et al. 2004). Their space density has been suggested to be about 40 times higher than that of bright galaxies (Staveley-Smith et al. 1992). Late-type dwarfs, dwarf irregular galaxies (dIrrs) and blue compact dwarf galaxies (BCDs), are galaxies harboring active or recent star formation activity, but have low metallicities, large

gas content and mostly young stellar populations. All these features indicate that they are poorly evolved objects, either newly formed galaxies or evolving slowly over the Hubble time. Especially BCDs, the least chemically evolved star-forming galaxies known in the universe ( $12+\log(\text{O}/\text{H})$  ranging between 7.1 and  $\sim 8.4$ ), are excellent laboratories for studying nucleosynthesis processes in a metal-deficient environment, in conditions similar to those prevailing at the time of galaxy formation (Thuan et al. 1995; Izotov & Thuan 1999). The study of the variations of one chemical element relative to another in these poorly evolved star-forming galaxies is crucial for our understanding of the early chemical evolution of galaxies and for constraining models of stellar nucleosynthesis.

dIrrs are dominated by scattered bright HII regions in the optical, while in HI they show a complicated fractal-like pattern of shells, filaments and clumps. Typical HI masses are  $\leq 10^9 M_\odot$ .

BCDs are currently undergoing an intense burst of star formation which gives birth to a large number ( $10^3 -$

$10^4$ ) of massive stars in a compact region ( $\leq 1$  kpc), which ionizes the interstellar medium, producing high-excitation supergiant HII regions and enriching it with heavy elements (Thuan et al. 1995). Part of the extended neutral gas may be kinematically decoupled from the galaxies (van Zee et al. 1998). The majority of BCDs (more than 99%) are not primordial systems, but evolved dwarf galaxies where starburst activity is immersed within an old extended stellar host galaxy (Kunth et al. 1988; Papaderos et al. 1996; Thuan 2008). However, recent work lends strong observational support to the idea that some among the most metal-deficient star-forming galaxies known in the local universe have formed most of their stellar mass within the last 1 Gyr, hence they qualify as young galaxy candidates (Papaderos et al. 2002; Izotov & Thuan 2004b; Pustilnik et al. 2004; Aloisi et al. 2007).

Searle et al. (1973) concluded that extremely blue galaxies should have undergone intense bursts of star formation (SF) separated by long quiescent periods (bursting SF). Recent detections of old underlying stellar populations in most BCDs seem to corroborate their suggestion and reveal at least another burst of SF besides the present one, even in the case of the most metal-poor BCDs known, I Zw 18 (Östlin 2000) and SBS 0335-052W (Lipovetsky et al. 1999).

Aside from the bursting SF mode, gasping (Tosi et al. 1991) or mild continuous (Carigi et al. 1999; Legrand 2000; Legrand et al. 2000) SF regimes have been proposed for dIrrs and BCDs. The gasping scenario, in which the interburst periods are significantly shorter than the active phases, is probably the more realistic picture for many of them (Schulte-Ladbeck et al. 2001).

It is very likely that dIrrs and BCDs have suffered galactic winds. In the past years, theorists have argued that winds carry heavy elements out of galaxies, and that they remove a larger fraction of the metals in lower mass galaxies (Larson 1974; Dekel & Silk 1986; De Young & Gallagher 1990; Mac Low & Ferrara 1999). The observational evidence of outflows from dwarf galaxies has grown rapidly in time (e.g., Meurer et al. 1992; Martin 1996; Bomans et al. 1997). Only recently, however, has it become possible to directly measure the metal content of galactic winds and confirm that winds are indeed metal enhanced (e.g., Martin et al. 2002).

In the past years many models for the chemical evolution of these galaxies appeared and tried to explain the intrinsic spread observed in their properties (Matteucci & Chiosi 1983; Matteucci & Tosi 1985; Pilyugin 1993; Marconi et al. 1994; Bradamante et al. 1998; Henry et al. 2000; Lanfranchi & Matteucci 2003; Romano et al. 2006). Most of these papers suggested that the spread can be reproduced by varying the efficiency of star formation or galactic wind from galaxy to galaxy or by assuming that there is self-pollution in the HII regions where the abundances are measured (Pilyugin 1993). Metal-enhanced winds with different prescriptions were studied (Marconi et al. 1994; Bradamante et al. 1998; Recchi et al. 2001, 2004; Romano et al. 2006).

Besides the chemical abundances, the photometric and spectral properties are also taken into account in some theoretical works (e.g., Vázquez et al. 2003; Stasińska & Izotov 2003; Martín-Manjón et al. 2008, 2009). Martín-Manjón et al. (2008, 2009) combined dif-

ferent codes of chemical evolution, evolutionary population synthesis and photoionization, and concluded that the closed box models with an attenuated bursting SF and a initial star formation efficiency (SFE)  $\epsilon = 0.1 \sim 0.3$  can reproduce the observed abundances, diagnostic diagrams and equivalent width-colour relations of local H II galaxies.

In this work, we present a new series of chemical evolution models for dIrrs and BCDs. The models are based on the original one of Bradamante et al. (1998), but consider a larger number of chemical species and updated stellar yields. We have tested both the bursting and the continuous regime of star formation. By comparing our model results with the most recent data of dIrrs and Damped Lyman- $\alpha$  systems (DLAs), we aim at understanding the importance of galactic winds, the history of star formation and the origin of the mass-metallicity relation in dwarf irregulars. A comparison between the properties of local dIrrs and those of high redshift DLAs will allow us to understand the nature of DLAs and establish whether they can be considered as the progenitors of local dIrrs and BCDs. Moreover, by studying in detail the abundance patterns such as  $[X/Fe]$  versus  $[Fe/H]$  will allow us to understand if these dwarf galaxies can be the building blocks of more massive galaxies, as suggested by the hierarchical clustering scenario of galaxy formation.

This paper is organized as follows. In Section 2, we present the observational constraints. In Section 3, the adopted chemical evolution models are described. Our model results are presented in details in Section 4 and discussed in Section 5.

## 2. Observational Properties

The metallicity, defined as the fraction of elements other than hydrogen and helium by mass, is an important indicator of the formation and evolutionary stage of a galaxy, and usually correlates with macroscopic properties of late-type galaxies, e.g. luminosity, mass, gas fraction, rotation speed, morphological type, etc. (e.g., Garnett 2002; Pilyugin et al. 2004; Lee et al. 2006; Vaduvescu et al. 2007). Except hydrogen and helium, oxygen is the most abundant element in the universe and easy to be measured in HII regions because of its bright emission lines. In practice, the oxygen abundance is usually used to represent the metallicity of the galaxy.

### 2.1. Luminosity-Metallicity ( $L - Z$ ) relation and Mass-Metallicity ( $M - Z$ ) relation

The strong correlation between the metallicity  $Z$  and the luminosity  $L$  of a galaxy is a robust relationship, holding over 10 mag in galaxy optical luminosity and a factor of 100 in metallicity (e.g., Garnett & Shields 1987; Zaritsky et al. 1994; Lamareille et al. 2004; Tremonti et al. 2004). Lequeux et al. (1979) have shown first the existence of the correlation between the metallicity and the mass in both compact and irregular galaxies, then confirmed by Skillman et al. (1989) who found that more luminous (or more massive) galaxies are more metal rich. The correlation is also found in spirals and elliptical galaxies (e.g., Garnett & Shields 1987; Brodie & Huchra 1991; Zaritsky et al. 1994; van Zee et al. 1997; Tremonti et al. 2004; Lee et al. 2006; Vaduvescu et al. 2007). Since the luminosity of a galaxy closely relates to its stellar mass, the

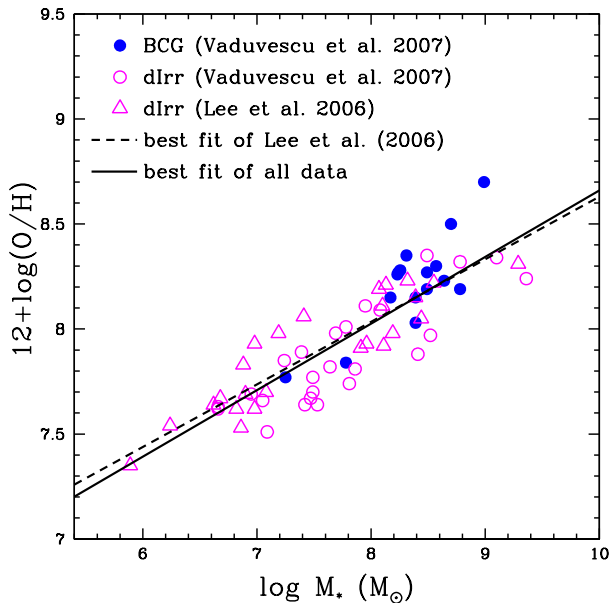


**Fig. 1.** Oxygen abundance vs. stellar mass for nearby dIrrs and BCDs. *Blue filled* and *magenta open circles* are data from Vaduvescu et al. (2007), and represent BCDs and dIrrs respectively; *magenta open triangles* are dIrrs observed by Lee et al. (2006), and the *dashed line* shows the best fit of their data. The *solid line* is the best linear fit of all data.

$L - Z$  relation should represent also the mass-metallicity relation. But how the luminosity is representative of stellar mass it depends on the frequency band one investigates. Traditionally, the  $L - Z$  relation is studied at optical wavelengths (e.g., Lequeux et al. 1979; Skillman et al. 1989, 1997; Pilyugin 2001; Garnett 2002; Lee et al. 2003a,b; Pilyugin et al. 2004; van Zee & Haynes 2006; Ekta & Chengalur 2010). The optical luminosity could be affected by the current star formation process, therefore more and more efforts were put into the determination of the near-infrared  $L - Z$  (and hence  $M_* - Z$ ) relation where the dominant emission arises from the older stellar populations (e.g., Pérez-González et al. 2003; J.C. Lee et al. 2004; Salzer et al. 2005; Lee et al. 2006; Mendes de Oliveira et al. 2006; Rosenberg et al. 2006; Vaduvescu et al. 2007; Saviane et al. 2008). Lee et al. (2006) considered 27 nearby star-forming dwarf irregular galaxies whose masses spread over 3 dex, and examined the  $M_* - Z$  relation at  $4.5 \mu\text{m}$  (*Spitzer*) (see Fig. 1). Vaduvescu et al. (2005, 2006, 2007) studied the properties of both dIrrs and BCDs, and obtained the  $M_* - Z$  relation by assuming  $M_*/L_K = 0.8 M_\odot/L_{K\odot}$ . They concluded that, for both dIrrs and BCDs, metallicity correlates with stellar mass, gas mass, and baryonic mass, in the sense that more massive systems are more metal-rich.

## 2.2. Gas fraction-metallicity ( $\mu - Z$ ) relation

A more useful relation for chemical evolution studies is the metallicity-gas fraction ( $\mu - Z$ ) relation, because it provides the information about how the gas convert into stars and metals, and also about gas flows (infall and/or outflow),

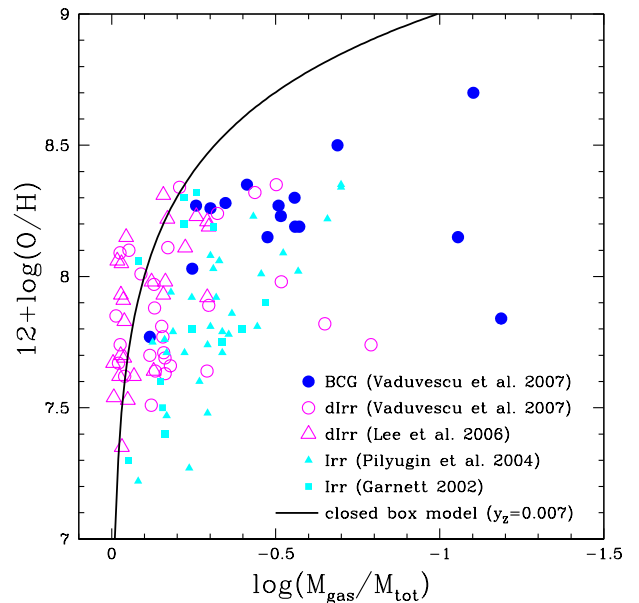


**Fig. 2.** Oxygen abundance vs. gas fraction relation for nearby dIrrs and BCDs. *Blue filled* and *magenta open circles* are data from Vaduvescu et al. (2007), and represent BCDs and dIrrs respectively; *magenta open triangles* are dIrrs observed by Lee et al. (2006); *cyan filled triangles* and *squares* are the Irrs observed by Pilyugin et al. (2004) and Garnett (2002) respectively. The *solid line* is the prediction of the closed box model ( $Z = y_Z \ln \mu^{-1}$ ) with an effective yield  $y_Z = 0.007$  corresponding to the Salpeter IMF and Woosley & Weaver (1995) nucleosynthesis.

as first suggested by Matteucci & Chiosi (1983) in their chemical evolution models of dwarf irregular galaxies.

As former works have shown, if the system does not have gas flows, the metallicity evolution predicted by the closed box model is a simple function of the gas fraction  $\mu$  and true yield  $y$  under the instantaneous recycling assumptions,  $Z = y_Z \ln(\mu^{-1})$  (Schmidt 1963; Searle & Sargent 1972). By comparing the “observed” effective yield,  $y_{Z,eff} = Z_{obs}/\ln(\mu_{obs}^{-1})$  with the true measured yield  $y_Z$ , one can understand whether the system evolved as a closed box or if infall and/or outflow have been important. In fact, both infall and outflow have the effect of decreasing the effective yield.

Lee et al. (2003a,b) showed that the oxygen abundance is tightly correlated with the gas fraction in dwarf irregular galaxies through optical observations, and they argued that these dIrrs have evolved in relative isolation, without inflow or outflow of gas. Lately, Lee et al. (2006) measured the  $4.5 \mu\text{m}$  luminosities for 27 nearby dIrrs with the *Spitzer* Infrared Array Camera, and showed the relation between oxygen abundances and gas-to-stellar mass ratio. Their results suggest reduced yields and/or significant outflow rates, which have been also indicated by previous authors (e.g., Garnett 2002; van Zee & Haynes 2006). Using NIR photometry, the most important discovery of Vaduvescu et al. (2007) is that the  $\mu - Z$  relation for BCDs follows that of dIrrs, and agrees with Lee et al. (2003a,b) that the evolution of field dIrrs has not been noticeably influenced by gas flows. However, they also point out that several dIrrs and at least one BCD do show HI deficiencies

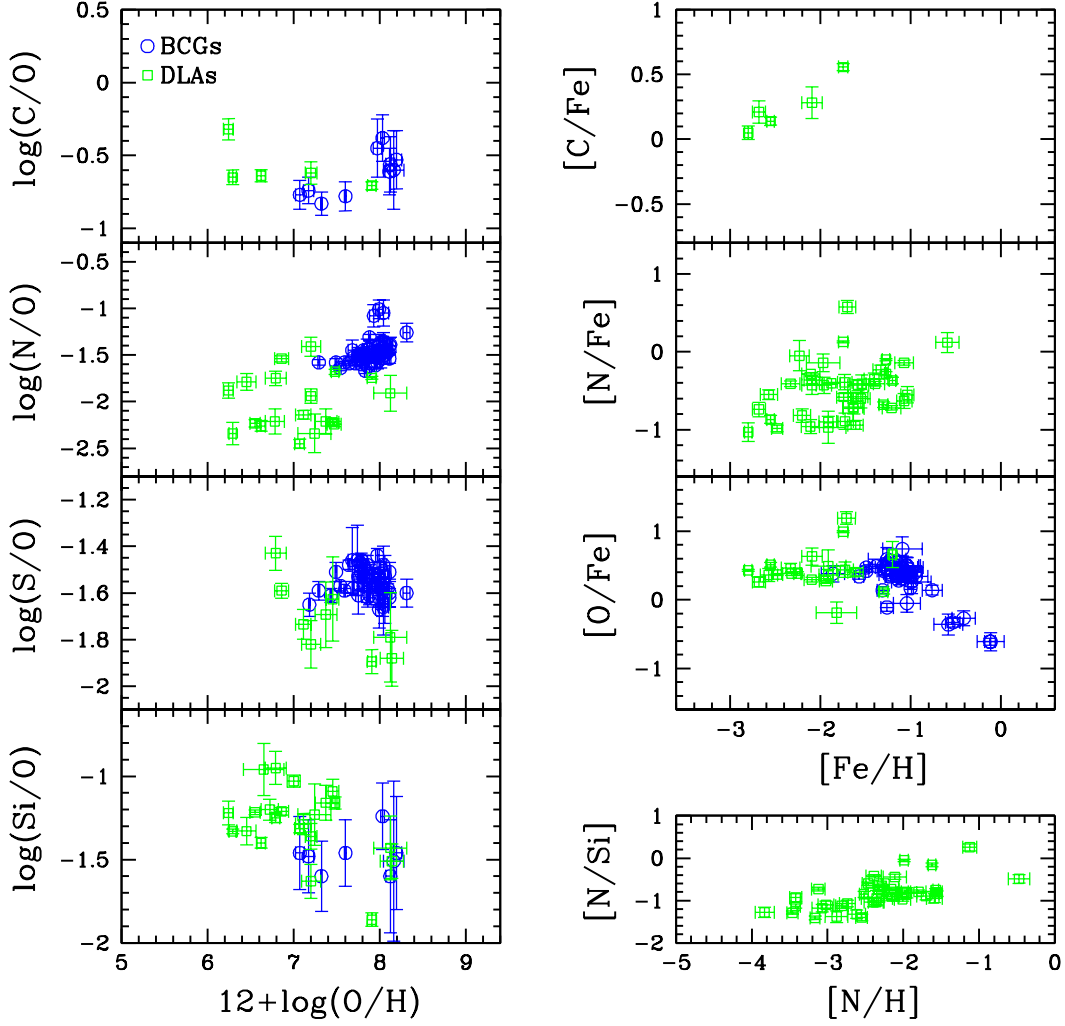


**Fig. 3.** Abundance ratio of different elements. *Blue open circles* are BCDs, from Izotov & Thuan (1999) and Papaderos et al. (2006); *green open squares* are DLAs, the data are shown in Table 1.

in dense environments, indicating that the gas may be removed by external processes. Using the effective yield as the only criterion for gas flow is too simplistic and the conclusion might not be reliable. Convincing conclusions should be reached through detailed modeling work.

In Fig. 2, we show the observed oxygen abundance-gas fraction relation of nearby dIrrs and BCDs. From this figure we can see, the BCDs have larger abundance and gas fraction range, while most dIrrs have higher gas fraction compared with BCDs and Irrs, implying their poorly evolved stages.

### 2.3. Abundance ratios

How the abundances of chemical elements change relative to one another is a crucial clue for understanding the chemical evolution of galaxies and stellar nucleosynthesis.

HII regions are ionized by newly born massive stars, hence showing the metallicity of the ISM at the present time. Therefore, metallicities in dIrrs and BCDs are usually derived from the ionized gas in HII regions through

their strong narrow emission lines. Izotov & Thuan (1999) presented high-quality ground-based spectroscopic observations of 54 supergiant HII regions in 50 low-metallicity BCDs with oxygen abundances  $12 + \log(O/H)$  between 7.1 and 8.3, and determined abundances for the elements N, O, Ne, S, Ar, Fe, and also C and Si in a subsample of 7 BCDs. Papaderos et al. (2006) presented spectroscopic and photometric studies of nearby BCDs in the 2dFGRS (Two-Degree Field Galaxy Redshift Survey), and measured their Ne/O, Fe/O and Ar/O ratios. Both of these works do not consider the dust depletion correction. We show the data of Izotov & Thuan (1999) and Papaderos et al. (2006) in Fig. 3.

DLA absorption systems, found in the spectra of high-redshift QSOs, are neutral clouds with large HI column densities,  $N(\text{HI}) \geq 2 \cdot 10^{20} \text{cm}^{-2}$ . They are likely to be protogalactic clumps embedded in dark matter halos and may provide the important information on the early chemical evolution of galaxies. With high resolution spectroscopy of QSO absorption lines, elemental abundances can be measured up to redshift  $z \approx 5$ . The chemical abun-

**Table 1.** The abundances of DLAs

QSO name	$z_{abs}$	dv(km/s)	ref.	$\log N_{HI}$	ref.	[C/H]	[N/H]	[O/H]	[Si/H]	[S/H]	[Fe/H]	ref.
1331+170	1.7764	75	1	$21.14 \pm 0.08$	2		$-2.390 \pm 0.128$		$-1.350 \pm 0.081$		$-1.960 \pm 0.085$	2,3
2230+025	1.8642	59	4	$20.83 \pm 0.05$	5		$-1.588 \pm 0.105$		$-0.641 \pm 0.071$		$-1.035 \pm 0.071$	5
2314-409	1.8750	59	4	$20.10 \pm 0.20$	5			$-2.010 \pm 0.233$	$-1.820 \pm 0.224$		$-1.820 \pm 0.224$	5
1210+1731	1.8918	62	1	$20.63 \pm 0.08$	6		$-1.700 \pm 0.120$		$-0.810 \pm 0.085$		$-1.070 \pm 0.085$	7
2206-199A	2.0762	20	1	$20.43 \pm 0.04$	8	$-2.410 \pm 0.050$	$-3.420 \pm 0.064$	$-2.040 \pm 0.050$	$-2.290 \pm 0.041$		$-2.550 \pm 0.041$	8
1444+014	2.0870	294	1	$20.25 \pm 0.07$	1		$-1.124 \pm 0.092$		$-1.380 \pm 0.092$		$-1.700 \pm 0.092$	9
1037-2703	2.1390			$19.70 \pm 0.10$	10		$-0.470 \pm 0.141$		$0.020 \pm 0.102$		$-0.590 \pm 0.128$	10
0528-2505	2.1410	105	1	$20.95 \pm 0.05$	11		$-2.150 \pm 0.094$		$-1.240 \pm 0.071$		$-1.550 \pm 0.103$	11
2348-147	2.2790	55	1	$20.59 \pm 0.08$	7		$-3.021 \pm 0.106$		$-1.921 \pm 0.094$		$-2.203 \pm 0.094$	6
2036-0553	2.2803			$21.20 \pm 0.15$	12		$-2.110 \pm 0.153$		$-1.670 \pm 0.158$		$-1.970 \pm 0.186$	12
0100+130	2.3090	37	1	$21.37 \pm 0.08$	2		$-2.120 \pm 0.128$				$-1.730 \pm 0.081$	2
2243-6031	2.3300	173	1	$20.67 \pm 0.02$	13		$-1.570 \pm 0.036$	$-0.540 \pm 0.191$	$-0.820 \pm 0.028$	$-0.810 \pm 0.036$	$-1.200 \pm 0.036$	13
1232+0815	2.3377	85	1	$20.80 \pm 0.10$	11		$-1.950 \pm 0.128$		$-1.130 \pm 0.135$		$-1.540 \pm 0.128$	11
1435+5359	2.3427			$21.05 \pm 0.10$	12		$-2.160 \pm 0.102$		$-1.430 \pm 0.102$			12
0841+129	2.3745	37	1	$21.00 \pm 0.10$	11		$-2.160 \pm 0.104$		$-1.302 \pm 0.108$		$-1.580 \pm 0.108$	7,11
0027-1836	2.4020			$21.75 \pm 0.10$	14		$-2.280 \pm 0.215$		$-1.590 \pm 0.128$		$-2.230 \pm 0.108$	14
0112-306	2.4191	31	1	$20.50 \pm 0.08$	15		$-3.120 \pm 0.089$	$-2.210 \pm 0.113$	$-2.389 \pm 0.082$		$-2.570 \pm 0.094$	9,15,16
2343+1232	2.4313	289	1	$20.40 \pm 0.07$	17		$-1.560 \pm 0.076$		$-0.760 \pm 0.092$		$-1.330 \pm 0.086$	17
1409+0930	2.4562	69	1	$20.54 \pm 0.04$	18			$-1.870 \pm 0.045$	$-1.970 \pm 0.045$		$-2.250 \pm 0.045$	16,18
1223+178	2.4661	91	1	$21.40 \pm 0.10$	15		$-2.350 \pm 0.205$		$-1.406 \pm 0.104$		$-1.640 \pm 0.112$	9,15,19
0841+129	2.4764	30	1	$20.78 \pm 0.08$	6		$-2.618 \pm 0.120$	$-1.287 \pm 0.128$	$-1.296 \pm 0.085$	$-1.460 \pm 0.128$	$-1.726 \pm 0.094$	6
1337+1121	2.5079	32	1	$20.12 \pm 0.05$	16		$-3.060 \pm 0.112$	$-1.880 \pm 0.112$				16
2344+12	2.5379	69	1	$20.32 \pm 0.07$	20		$-2.321 \pm 0.076$		$-1.580 \pm 0.076$		$-1.740 \pm 0.077$	1,19
0405-443	2.5505	165	1	$21.13 \pm 0.10$	21		$-2.360 \pm 0.104$		$-1.320 \pm 0.108$		$-1.630 \pm 0.117$	21
1558+4053	2.5533			$20.30 \pm 0.04$	8	$-2.470 \pm 0.072$	$-3.420 \pm 0.081$	$-2.420 \pm 0.057$	$-2.490 \pm 0.072$		$-2.680 \pm 0.072$	8
0405-443	2.5950	79	1	$21.09 \pm 0.10$	21		$-1.800 \pm 0.102$		$-1.010 \pm 0.104$		$-1.390 \pm 0.102$	21
0913+072	2.6184	22	1	$20.34 \pm 0.04$	8	$-2.750 \pm 0.064$	$-3.830 \pm 0.126$	$-2.370 \pm 0.041$	$-2.550 \pm 0.041$		$-2.800 \pm 0.041$	8
0405-443	2.6215	182	1	$20.47 \pm 0.10$	21			$-1.940 \pm 0.102$	$-1.990 \pm 0.117$		$-2.320 \pm 0.102$	21
1759+7539	2.6250	74	22	$20.76 \pm 0.01$	23		$-1.555 \pm 0.027$		$-0.720 \pm 0.061$		$-1.274 \pm 0.014$	23,24
0812+32	2.6260	70	22	$21.35 \pm 0.10$	25			$-0.520 \pm 0.135$	$-0.880 \pm 0.112$	$-0.880 \pm 0.128$	$-1.710 \pm 0.100$	26
1409+0930	2.6682	36	4	$19.70 \pm 0.04$	18		$-1.980 \pm 0.045$	$-1.180 \pm 0.045$	$-1.190 \pm 0.050$		$-1.300 \pm 0.050$	16,18
1558-0031	2.7026			$20.67 \pm 0.05$	27		$-1.990 \pm 0.054$	$-1.460 \pm 0.112$	$-1.940 \pm 0.054$	$-1.760 \pm 0.054$		8,12
1337+1121	2.7957	42	1	$20.95 \pm 0.10$	25		$-2.740 \pm 0.104$	$-1.870 \pm 0.122$	$-1.670 \pm 0.122$	$-1.780 \pm 0.102$	$-2.330 \pm 0.102$	16,26
1426+6039	2.8268	136	22	$20.30 \pm 0.04$	28		$-1.370 \pm 0.041$				$-1.270 \pm 0.041$	26
1946+7658	2.8443	22	4	$20.27 \pm 0.06$	28		$-3.462 \pm 0.072$	$-2.110 \pm 0.061$	$-2.176 \pm 0.061$		$-2.478 \pm 0.061$	19
2342+3417	2.9082	100	22	$21.15 \pm 0.10$	25		$-2.010 \pm 0.108$		$-1.040 \pm 0.102$		$-1.580 \pm 0.117$	26
1021+3001	2.9490	70	22	$20.70 \pm 0.10$	25		$-3.070 \pm 0.135$		$-1.890 \pm 0.102$		$-2.110 \pm 0.100$	26
0001	3.0000	75	4	$20.70 \pm 0.05$	19		$-3.165 \pm 0.064$	$-1.594 \pm 0.055$	$-1.758 \pm 0.051$			19
0741+4741	3.0174	42	22	$20.48 \pm 0.10$	26		$-2.283 \pm 0.100$		$-1.636 \pm 0.100$		$-1.878 \pm 0.100$	19
0347-383	3.0250	93	1	$20.73 \pm 0.05$	1	$-1.191 \pm 0.055$	$-1.620 \pm 0.051$	$-0.754 \pm 0.051$	$-1.464 \pm 0.064$	$-1.128 \pm 0.071$	$-1.748 \pm 0.051$	9,15,29
2332-0924	3.0572	111	1	$20.50 \pm 0.07$	16		$-2.550 \pm 0.076$	$-1.210 \pm 0.073$	$-1.150 \pm 0.099$	$-1.316 \pm 0.193$	$-1.610 \pm 0.086$	9,16,15,25
2059-360	3.0830	44	1	$20.98 \pm 0.08$	15		$-2.810 \pm 0.082$	$-1.550 \pm 0.089$	$-1.687 \pm 0.094$	$-1.764 \pm 0.094$	$-1.910 \pm 0.106$	15,16,30
1340+136	3.1180	153	1	$20.05 \pm 0.08$	16		$-2.550 \pm 0.082$	$-1.190 \pm 0.082$				16
0930+2858	3.2350	26	22	$20.35 \pm 0.10$	25		$-2.390 \pm 0.101$		$-1.972 \pm 0.102$		$-2.105 \pm 0.101$	19
0900+4215	3.2458	95	4	$20.30 \pm 0.10$	26		$-1.930 \pm 0.102$				$-1.210 \pm 0.102$	12,26
0201+1120	3.3848	67	22	$21.30 \pm 0.10$	31		$-1.750 \pm 0.117$				$-1.400 \pm 0.113$	19,32
0000-263	3.3901	33	1	$21.41 \pm 0.08$	28		$-2.460 \pm 0.085$	$-1.800 \pm 0.081$	$-1.860 \pm 0.082$	$-1.870 \pm 0.085$	$-2.095 \pm 0.085$	28,33
1108-0747	3.6080	31	1	$20.37 \pm 0.07$	1			$-1.660 \pm 0.076$	$-1.540 \pm 0.073$		$-1.936 \pm 0.071$	1,16,26
1443+2724	4.2240	130	1	$20.95 \pm 0.10$	1		$-1.210 \pm 0.100$				$-1.070 \pm 0.104$	1
1202-0725	4.3829	170	22	$20.55 \pm 0.03$	34	$-1.810 \pm 0.058$	$-2.520 \pm 0.058$	$-1.460 \pm 0.067$	$-1.670 \pm 0.058$		$-2.092 \pm 0.114$	28,34
0307-4945	4.4660	192	22	$20.67 \pm 0.09$	35		$-2.880 \pm 0.150$	$-1.420 \pm 0.192$	$-1.500 \pm 0.114$		$-1.910 \pm 0.192$	35

**References.** (1)Ledoux et al. (2006); (2)Dessauges-Zavadsky et al. (2004); (3)Kulkarni et al. (1996); (4)Abate et al. (2008); (5)Ellison & Lopez (2001); (6)Dessauges-Zavadsky et al. (2006); (7)Dessauges-Zavadsky et al. (2007); (8)Pettini et al. (2008); (9)Ledoux et al. (2003); (10)Srianand & Petitjean (2001); (11)Centurión et al. (2003); (12)Henry & Prochaska (2007); (13)Lopez et al. (2002); (14)Noterdaeme et al. (2008); (15)Srianand et al. (2005); (16)Petitjean et al. (2008); (17)Noterdaeme et al. (2007); (18)Pettini et al. (2002); (19)Prochaska et al. (2002a); (20)Péroux et al. (2006); (21)Lopez & Ellison (2003); (22)Prochaska et al. (2008); (23)Outram et al. (1999); (24)Prochaska et al. (2002b); (25)Prochaska et al. (2003); (26)Prochaska et al. (2007); (27)O’Meara et al. (2006); (28)Lu et al. (1996); (29)Levshakov et al. (2002); (30)Petitjean et al. (2000); (31)Storrie-Lombardi & Wolfe (2000); (32)Ellison et al. (2001); (33)Molaro et al. (2001); (34)D’Odorico & Molaro (2004); (35)Dessauges-Zavadsky et al. (2001).

dances of DLA systems give us complementary observational constraints on the formation and evolution of galaxies. Abundance measurements in DLA systems relevant for the present work are listed in Table 1 and plotted in Fig. 3 (green squares). In comparing DLA abundances with model predictions care must be taken for dust depletion effects. Luckily, these effects are expected to be negligible for most of the elements used in the present investigation, such as C, N, O and S: in fact these elements show little values of depletion, if any, in nearby interstellar clouds (Jenkins 2009) and are expected to be even less depleted in DLA systems. On the other hand, we expect some depletion effects for Fe and, to a lesser extent, for Si. Estimates of Fe depletion in DLAs based on the comparison with Zn measurements (Vladilo 2004) are available only for a few systems of Table 1. These results indicate that Fe tend to be underestimated when the level of metallicity is relatively high. This explain the few cases with largest deviations from BCD measurements and from the model predictions shown in Figs. 3, 5, 8, 10, 11, 13, and 17.

#### 2.4. Primordial helium abundance $Y_p$ and $\Delta Y/\Delta Z$

The determination of primordial helium abundance,  $Y_p$ , is important for the study of cosmology and the evolution of galaxies, because an accurate initial  $Y$  is required to test Big Bang nucleosynthesis and build chemical evolution models.

One way of estimating  $Y_p$  is by extrapolating the observed helium-metallicity ( $Y - Z$ ) relation to  $Z = 0$  by assuming the slope  $\Delta Y/\Delta Z$  to be constant. More recently, it has been common practice to use  $\Delta Y/\Delta O$  since the oxygen abundance is easier to determine and can represent the metals. To obtain an accurate  $Y_p$  value, a reliable determination of  $\Delta Y/\Delta O$  for oxygen-poor objects is needed (e.g., Izotov et al. 1999; A. Peimbert 2003; Luridiana et al. 2003; Izotov & Thuan 2004a; M. Peimbert 2007). Izotov & Thuan (2004a) derived the primordial helium  $Y_p = 0.2429 \pm 0.0009$  and the slope  $\Delta Y/\Delta O = 4.3 \pm 0.7$  from observations of 82 HII regions. For a restricted sample (7 HII regions), they obtained  $Y_p = 0.2421 \pm 0.0021$  and  $\Delta Y/\Delta O = 5.7 \pm 1.8$ . Later, Izotov et al. (2006) derived  $Y_p = 0.2463 \pm 0.0030$  from the emission of the whole HII region of the extremely metal-deficient blue compact dwarf galaxy SBS 0335 – 052E. M. Peimbert (2007) has adopted  $\Delta Y/\Delta O = 3.3 \pm 0.7$  from theoretical and observational results, and derived  $Y_p = 0.2474 \pm 0.0029$ . These values are in excellent agreement with the value derived by Spergel et al. (2007) from the WMAP results,  $Y_p = 0.2482 \pm 0.0004$ .

In Fig. 4 we replot the helium-oxygen abundance relation of Izotov & Thuan (2004a) by using their data in Table 5. The linear regression is the one derived from the whole sample  $Y = 0.2429 + 43 * (O/H)$ .

### 3. Model Prescriptions

In this work, we used an updated version of the chemical evolution model developed by Bradamante et al. (1998) to study the formation and evolution of late-type dwarf galaxies, dIrrs and BCDs.

The general picture is the following: our model is one-zone and assumes the galaxy built up by continuous infall

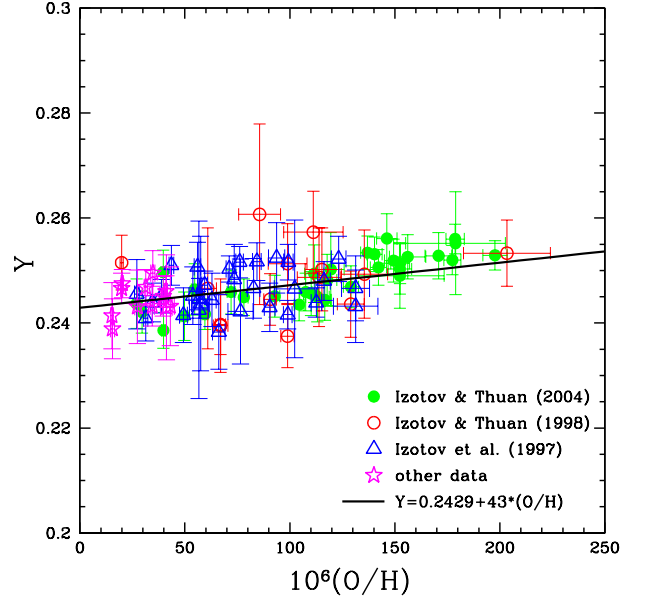


**Fig. 4.** Helium-metallicity ( $Y - Z$ ) relation for HII regions in BCDs, Fig. 2 of Izotov & Thuan (2004a). *Green filled circles*, from Izotov & Thuan (2004a); *red open circles*, from Izotov & Thuan (1998b); *blue open triangles*, from Izotov et al. (1997); *magenta open pentagrams*, from other data (Izotov & Thuan 1998a; Izotov et al. 1999; Thuan et al. 1999; Izotov et al. 2001a,b; Guseva et al. 2001, 2003a,b); the *solid line* is the maximum likelihood linear regression of all data,  $Y = 0.2429 + 43 * (O/H)$

of primordial gas ( $X = 0.7571$ ,  $Y_p = 0.2429$ ,  $Z = 0$ ). Stars form and then contaminate the interstellar medium (ISM) with their newly produced elements which mix with the ISM instantaneously and completely. Stellar lifetimes are taken into account in detail, i.e. the instantaneous recycling approximation (IRA) is relaxed. The energy released by supernovae (SNe) and stellar winds is partially deposited in the ISM, and galactic winds develop when the thermal energy of the gas exceeds its binding energy. The wind expels metals from the galaxy, hence it has a significant influence on the chemical enrichment of the galaxy.

The time evolution of the fractional mass of the element  $i$  in the gas,  $G_i$ , is described by the equations:

$$\dot{G}_i(t) = -\psi(t)X_i(t) + R_i(t) + \dot{G}_{i,inf}(t) - \dot{G}_{i,out}(t), \quad (1)$$

where  $G_i(t) = M_g(t)X_i(t)/M_L(t_G)$  is the gas mass in the form of an element  $i$  normalized to the total baryonic mass  $M_L$  at the present day  $t_G = 13$  Gyr;  $M_g(t)$  is the gas mass at time  $t$  and  $X_i(t)$  represents the mass fraction of element  $i$  in the gas, i.e., abundance by mass. The quantity  $G(t) = M_g(t)/M_L(t_G)$  represents the total fractional mass of gas and  $X_i(t)$  can be expressed by  $G_i(t)/G(t)$ . The four items on the right hand side of equation (1) show the mass change of the element  $i$  caused by the formation of new stars  $\psi(t)X_i(t)$ , the material returned through stellar winds or SN explosion  $R_i(t)$ , the infall of primordial gas  $\dot{G}_{i,inf}(t)$ , and the outflow  $\dot{G}_{i,out}(t)$  respectively.

The star formation rate (SFR)  $\psi(t)$  in this work is simply assumed as:

$$\psi(t) = \epsilon G(t), \quad (2)$$

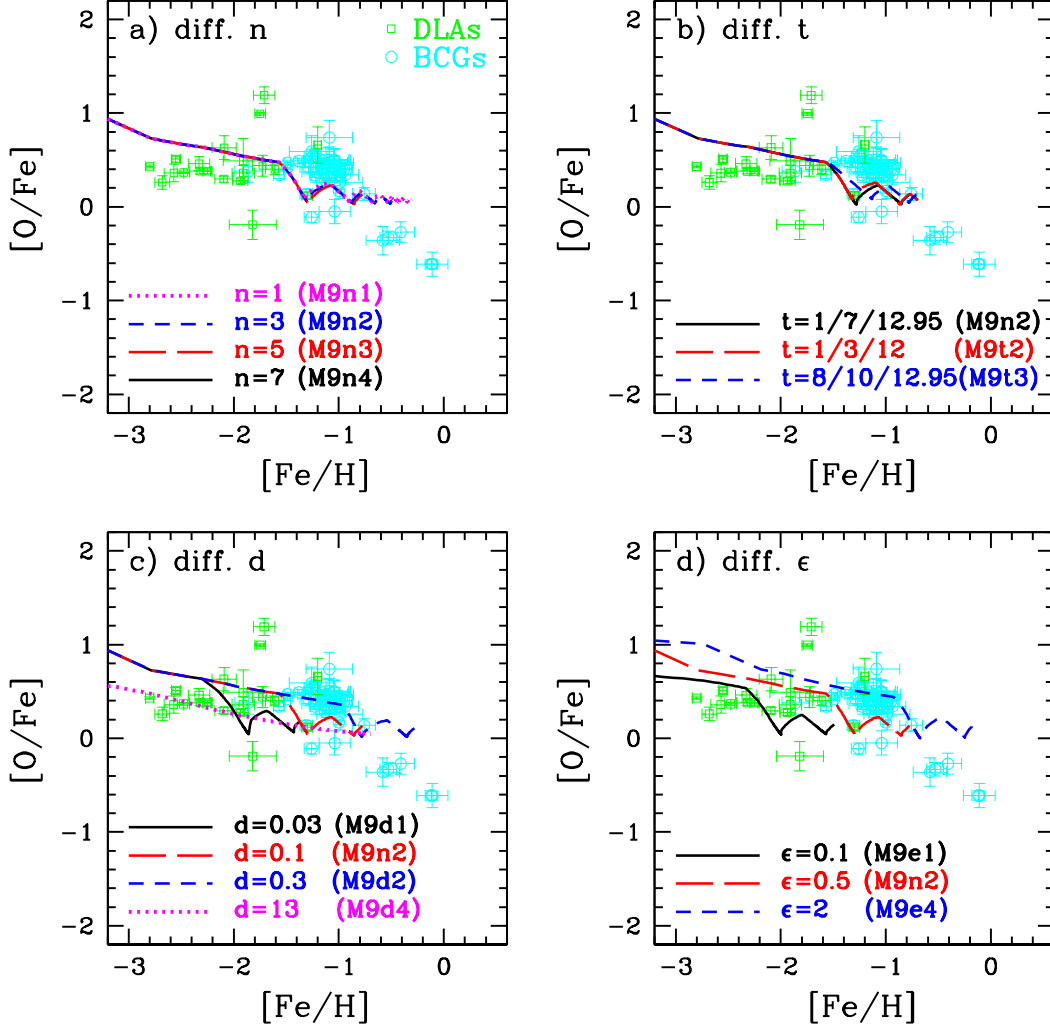


**Fig. 5.** The evolutionary tracks of  $[O/Fe]$  vs.  $[Fe/H]$  as predicted by models without outflow. a) models with different number of bursts; b) models with different occurrence times of bursts; c) models with different durations of bursts; d) models with different star formation efficiency. All these models assume the same total infall mass  $M_{infall} = 10^9 M_{\odot}$ . The cyan open circles are BCDs and green open squares are DLAs, same as in Fig. 3.

where  $\epsilon$  is the star formation efficiency and is in units of  $\text{Gyr}^{-1}$ , being one of the free parameters in our work.

The rate of gas infall is assumed to be exponentially decreasing with time:

$$f_{infall}(t) = Ae^{-t/\tau}, \quad (3)$$

where  $A$  is the normalization constant which is constrained by the boundary condition  $\int_0^{t_G} Ae^{-t/\tau} dt = 1$ , and  $\tau$  is the infall timescale. So we can easily obtain the accretion rate of an element  $i$  through the formula

$$\dot{G}_{i,infall}(t) = X_{i,infall} f_{infall} = \frac{X_{i,infall} e^{-t/\tau}}{\tau(1 - e^{-t_G/\tau})}, \quad (4)$$

$X_{i,infall} = 0$  ( $i \neq \text{H, He}$ ) if primordial gas is assumed.

In our model, the galactic wind develops when the thermal energy of the gas  $E_g^{th}(t)$  exceeds its binding energy  $E_g^b(t)$ :

$$E_g^{th}(t) \geq E_g^b(t). \quad (5)$$

The thermal energy of the gas is produced by SN explosions (both Type II and Type Ia) and stellar winds:

$$E_g^{th}(t) = E_{SNII}^{th}(t) + E_{SNIa}^{th}(t) + E_{sw}^{th}(t). \quad (6)$$

However, not all the energy produced in the above mentioned events is stored into the ISM, since a fraction of it is lost by cooling. In Bradamante et al. (1998)'s work, the efficiencies of energy transfer from SN and stellar winds into the ISM are the same,  $\eta_{SNII} = \eta_{SNIa} = \eta_{sw} = 0.03$  (see their work for more details). However, more recently, Recchi et al. (2001) and Recchi et al. (2002) have shown that since SN Ia explosions occur in a hotter and more rarefied medium, their energy can be more efficiently thermalized into the ISM and, consequently, their efficiency of energy transfer is higher. Therefore, in this work we assume that the efficiencies of energy transfer are  $\eta_{SNII} = 0.03$ ,  $\eta_{SNIa} = 0.8$  and  $\eta_{sw} = 0.03$  for SN II, SN Ia and stellar winds respectively.

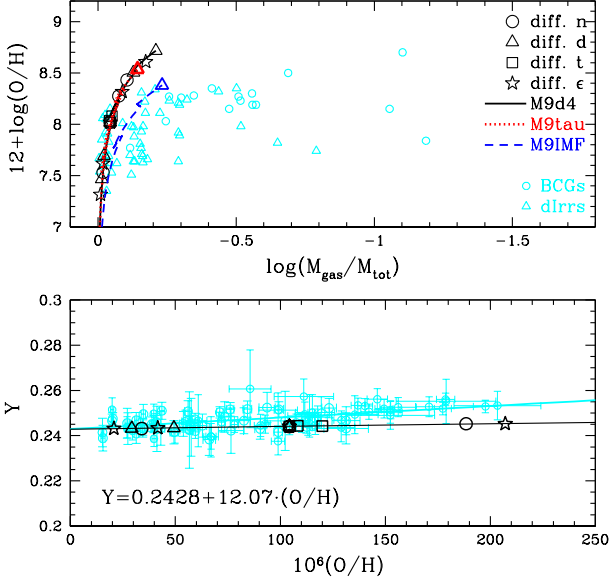


**Fig. 6.** Present oxygen abundance vs. gas fraction (*upper* panel) and  $Y$  vs. oxygen abundance (*lower* panel) as predicted by models without wind. All these models assume the same total infall mass  $M_{infall} = 10^9 M_{\odot}$ . *Big black open circles*: models with different numbers of bursts; *big black open triangles*: models with different durations of bursts; *big black open squares*: models with different occurrence times of bursts; *big black open pentacles*: models with different star formation efficiency. *Black solid*, *red dotted* and *blue-dash lines* in upper panel are the evolutionary tracks of model M9d4, M9tau and M9IMF. The *black-solid line* in lower panel is the best fit of all the model points. The observational data are the same as in Fig. 2 and Fig. 4, *cyan open circles* and *cyan open triangles* represent BCDs and dIrrs respectively. The *cyan solid line* is the best fit of the observational data.

To compute  $E_g^b(t)$ , the binding energy of gas, we also followed Bradamante et al. (1998) and assumed that each galaxy has a dark matter halo. The binding energy of gas is described as:

$$E_{Bgas}(t) = W_L(t) + W_{LD}(t) \quad (7)$$

with:

$$W_L(t) = -0.5 G \frac{M_{gas}(t)M_L(t)}{r_L} \quad (8)$$

which is the potential well due to the luminous matter and with:

$$W_{LD}(t) = -G_{wLD} \frac{M_{gas}(t)M_{dark}}{r_L} \quad (9)$$

which represents the potential well due to the interaction between dark and luminous matter, where  $w_{LD} \sim \frac{1}{2\pi} S(1 + 1.37S)$ , with  $S = r_L/r_D$ , being the ratio between the galaxy effective radius ( $r_L$ ) and the radius of the dark matter core ( $r_D$ ) (see Bertin et al. 1992). We assumed as in Bradamante et al. (1998) that the dark matter halo is 10 times more massive than the luminous matter and that  $S = 0.3$ .

The rate of gas loss via galactic wind for each element is assumed to be simply proportional to the amount of gas

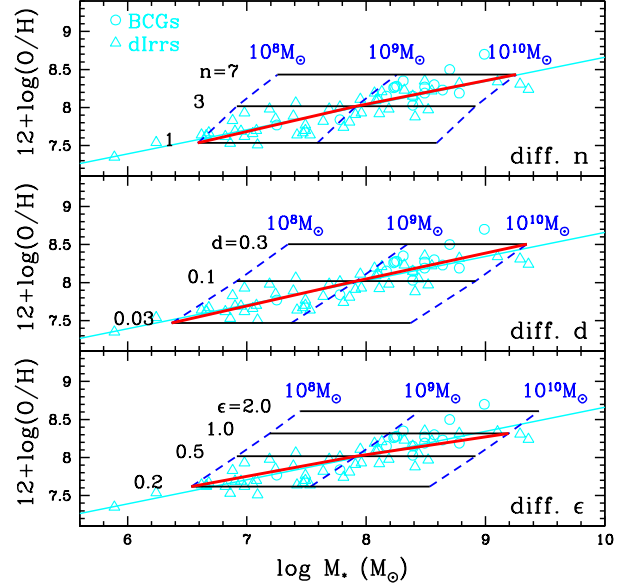


**Fig. 7.** Present day oxygen abundance vs.  $M_*$  as predicted by models without wind. The upper (middle/lower) panel shows the model results with different numbers of bursts (durations/SFE), along the *blue-dashed lines* the number of bursts (durations/SFE) increases from 2 to 7 (0.02 to 0.3/ 0.1 to 2), and along the *black-solid line* the total infall mass  $M_{infall}$  increases from  $10^8$  to  $10^{10} M_{\odot}$ . The *red-thick-solid line* connects the models which are consistent with the observational data, larger  $n$  ( $d/\epsilon$ ) for more massive galaxy. The observational data are the same as in Fig. 1, *cyan open circles* for BCDs and *cyan open triangles* for dIrrs.

present at the time  $t$ :

$$\dot{G}_{i,out}(t) = w_i \lambda G(t) X_{i,out}(t), \quad (10)$$

where  $X_{i,out}(t)$ , the abundance of the element  $i$  in the wind, is assumed to be same with  $X_i(t)$ , the abundance in the ISM;  $\lambda$  describes the efficiency of the galactic wind and has the same units as  $\epsilon$  ( $\text{Gyr}^{-1}$ );  $w_i$  is the efficiency weight of each element, hence  $w_i \lambda$  is the effective wind efficiency of the element  $i$ .  $\lambda$  and  $w_i$  are the other two free parameters in our model. In this work, we have studied two kinds of wind, the normal wind and the metal-enhanced wind. In the case of the normal wind, all elements are lost in the same way, i.e.,  $w_i = 1$  for all elements, and we use  $\lambda_w$  to denote the wind efficiency in this case; however, wind provoked by SN explosion could carry out more metals than H and He ( $w_i > w_{H,He}$ ,  $i \neq H, He$ ), which is the so-called “metal-enhanced” wind (Mac Low & Ferrara 1999; Recchi et al. 2001; Fujita et al. 2003; Recchi et al. 2008), and we use  $\lambda_{mw}$  to denote the wind efficiency in this case.

The initial mass function (IMF) is usually assumed to be constant both in space and time in different galaxies, and can be expressed as a power law of stellar mass as suggested first by Salpeter (1955):

$$\phi(m) = \phi_0 m^{-(1+x)}, \quad (11)$$

where  $x = 1.35$  for Salpeter IMF and  $\phi_0$  is the normalization constant which can be obtained by satisfying  $\int m \phi(m) dm = 1$  in the mass range  $0.1 - 100 M_{\odot}$ . However,

**Table 2.** Parameters of models without outflow

	Model name			SFE Gyr <sup>-1</sup>	$n$	$t^1$ Gyr	$d$ Gyr
	$10^8 M_\odot$	$10^9 M_\odot$	$10^{10} M_\odot$				
diff. n	M8n1	M9n1	M10n1	0.5	1	13	0.1*1
	M8n2	M9n2	M10n2	0.5	3	1/7/13	0.1*3
	M8n3	M9n3	M10n3	0.5	5	1/4/7/10/13	0.1*5
	M8n4	M9n4	M10n4	0.5	7	1/3/5/7/9/11/13	0.1*7
diff. d	M8d1	M9d1	M10d1	0.5	3	1/7/13	0.03*3
	M8d2	M9d2	M10d2	0.5	3	1/7/13	0.1*3
	M8d3	M9d3	M10d3	0.5	3	1/7/13	0.3*3
		M9d4		0.01	1	6.5	13
diff. t	M8t1	M9t1	M10t1	0.5	3	1/7/13	0.1*3
	M8t2	M9t2	M10t2	0.5	3	1/3/12	0.1*3
	M8t3	M9t3	M10t3	0.5	3	8/10/13	0.1*3
diff. $\epsilon$	M8e1	M9e1	M10e1	0.1	3	1/7/13	0.1*3
	M8e2	M9e2	M10e2	0.2	3	1/7/13	0.1*3
	M8e3	M9e3	M10e3	1.0	3	1/7/13	0.1*3
	M8e4	M9e4	M10e4	2.0	3	1/7/13	0.1*3
$\tau = 10$ Gyr		M9tau	0.5	3	1/7/13	0.5*3	
IMF <sub>scalo86</sub>		M9IMF	0.5	3	1/7/1	0.5*3	

**Notes.** <sup>(1)</sup> The middle time of the burst.

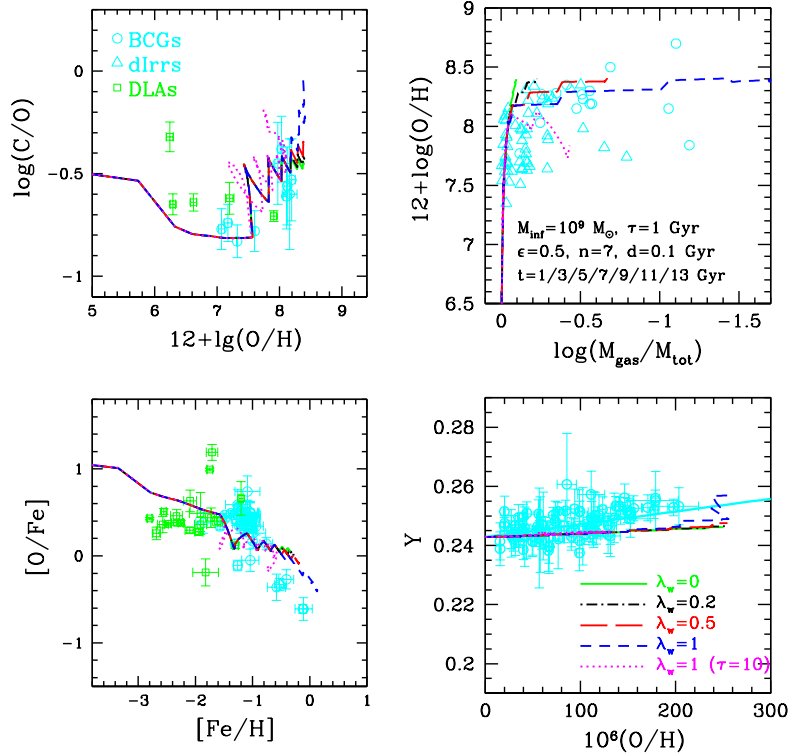


**Fig. 8.** The evolutionary track as predicted by models with normal wind. The left two panels are  $\log(\text{C}/\text{O})$  vs.  $12 + \log(\text{O}/\text{H})$  and  $[\text{O}/\text{Fe}]$  vs.  $[\text{Fe}/\text{H}]$ ; the right two panels are oxygen abundance vs. gas fraction and  $Y$  vs.  $(\text{O}/\text{H})$ . All the 5 models have same bursts sequence ( $\tau = 1$  Gyr,  $t = 1/3/5/7/9/11/13$  Gyr, and  $d = 0.1$  Gyr for each burst), but different wind efficiencies, *green-solid lines* for  $\lambda_w = 0$ , *black-dash-dot lines* for  $\lambda_w = 0.2$ , *red-long-dash lines* for  $\lambda_w = 0.5$ , and *blue-short-dash lines* for  $\lambda_w = 1$ . A model with long infall timescale ( $\tau = 10$  Gyr,  $\lambda_w = 1$ ) is shown in *magenta dotted line*. All these models assume the same total infall mass  $M_{\text{inf}} = 10^9 M_\odot$ . The observational data are the same as in Fig. 2, Fig. 3 and Fig. 4, BCDs, dIrrs, and DLAs are plotted in *cyan open circles*, *cyan open triangles* and *green open squares* here.

we tested also the Scalo (1986) IMF:

$$\phi_{\text{scalo86}}(m) \propto \begin{cases} m^{-2.35}, & (0.1 \leq m < 2) \\ m^{-2.7}, & (2 \leq m \leq 100). \end{cases} \quad (12)$$

which is a two-slope IMF and is steeper at the high mass end.

Stellar yields of different elements are important ingredients of chemical evolution studies. In this work, we adopt stellar yields of Woosley & Weaver (1995) for massive stars and van den Hoek & Groenewegen (1997) for low- and intermediate-mass stars. Both of them are metallicity-dependent.

#### 4. Model Results

In order to understand the observed global properties and abundance patterns of late-type dwarf galaxies, we have calculated several models. The typical galaxy is assumed to be forming by continuous infall of primordial gas and bursting star formation, as suggested by several previous works (e.g., Searle et al. 1973; Matteucci & Chiosi 1983; Marconi et al. 1994; Bradamante et al. 1998; Lanfranchi & Matteucci 2003; Romano et al. 2006). We also checked the case of continuous star formation for these galaxies (see Sect. 4.5).

##### 4.1. Model without outflow

Here we examine the models without outflow. Different numbers  $n$ , durations  $d$ , times of the occurrence of bursts  $t$ , and different star formation efficiencies  $\epsilon$  have been tested. The parameters adopted in the models are listed in Table 2. All the models assume short infall timescales ( $\tau = 1$  Gyr) except model M9tau, and the galactic lifetime is taken to be 13 Gyr for all the models. From the second to the fourth columns there are the model names, classified by different total infalling mass, from  $10^8 M_{\odot}$  to  $10^{10} M_{\odot}$ ; the fifth column shows the SFE; the sixth column the number of the bursts; the seventh column the middle time of each burst; the eighth column the duration of each burst, where “0.1\*3” means the duration of three bursts are the same, namely 0.1 Gyr.

In Fig. 5, we show the evolutionary tracks of  $[\text{O}/\text{Fe}]$  vs.  $[\text{Fe}/\text{H}]$  as predicted by models with a different number of bursts (panel a), different times for the occurrence of the bursts (panel b), different burst durations (panel c), and also different SFEs (panel d). The most distinctive feature of the bursting star formation scenario is the “saw-tooth” behaviour of the tracks, which is caused by the different origins of  $\alpha$ -elements and iron-peak elements. Oxygen is mainly synthesized by massive stars, therefore its abundance increases only during the bursting time, whereas iron is mainly synthesized by the Type Ia supernovae and its abundance still increases after the burst is over owing to the time delay of SN Ia explosions.

As we can see from Fig. 5, different durations of bursts and different SFEs among galaxies could be the explanation of the scatter in the data. In panel c, as a comparison, we also plot the model results for a low continuous star formation process (model M9d4). Clearly in this case the saw-tooth behaviour disappears.

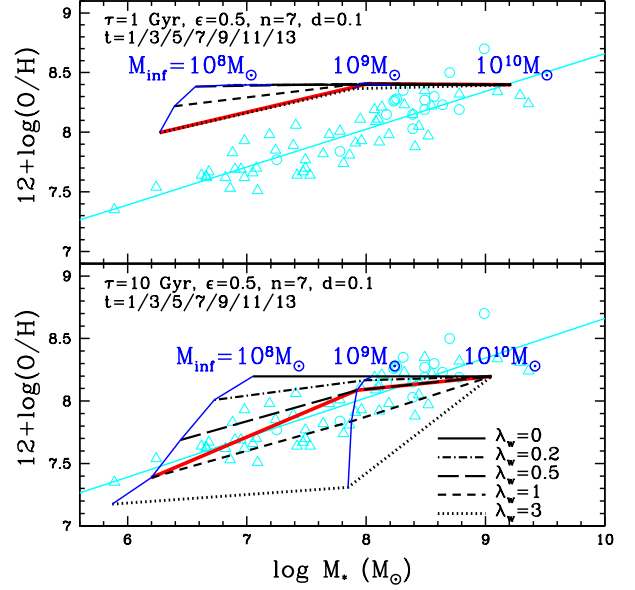


**Fig. 9.** Present day oxygen abundance vs.  $M_*$  as predicted by models with normal wind. All the models contain 7 bursts and the same burst sequence ( $\epsilon = 0.2, n = 7, t = 1/3/5/7/9/11/13, d = 0.1$  for each burst), and the total infall mass varies from  $M_{\text{inf}} = 10^8$  to  $10^{10} M_{\odot}$ . The upper panel shows results with short infall timescale ( $\tau = 1$  Gyr), whereas the lower one shows results with long timescale ( $\tau = 10$  Gyr). The predicted  $M - Z$  relation with different strength of normal wind are shown in black lines: *black solid, dash-dot, long-dash, short-dash, and dotted lines* are for  $\lambda_m = 0, 0.2, 0.5, 1, 3$  respectively. Models with same  $M_{\text{inf}}$  are connected by *blue lines*. An increasing wind efficiency to less massive galaxies is shown in *red-solid line*. Observational data are shown in *cyan open circles* (BCDs) and *cyan open triangles* (dIrrs), the *cyan solid line* is the best fit of all data, same as in Fig. 1.

If we compare the present oxygen abundance vs. the gas fraction as predicted by the above models with the observations (Fig. 6, upper panel), we can see that no matter how the star formation history changes (different  $n, t, d, \epsilon$ ), the model results always stay along the same curve. As first suggested by Matteucci & Chiosi (1983), in order to explain the spread in this diagram one should necessarily claim a variation of the IMF, or of the wind rate, or of the infall rate. Therefore, we examined the other IMF (Scalo 1986) which is steeper than Salpeter IMF at the massive end. However, the model results in Fig. 6 still cannot explain the observed lowest oxygen abundance at the same  $\mu$  or the lowest  $\mu$  at the same oxygen abundance. Therefore, unless one assumes unrealistically steeper IMFs, the observed  $\mu - Z$  strongly implies that there should have other mechanisms operating in the galaxy which can reduce the O abundance or the gas fraction.

In the lower panel of Fig. 6, it is shown the  $Y - (\text{O}/\text{H})$  relation as predicted by our model which is consistent with the observations, although a little flatter than the observed best fit. The best fit to these model results is  $Y = 0.2428 + 12.07(\text{O}/\text{H})$ .

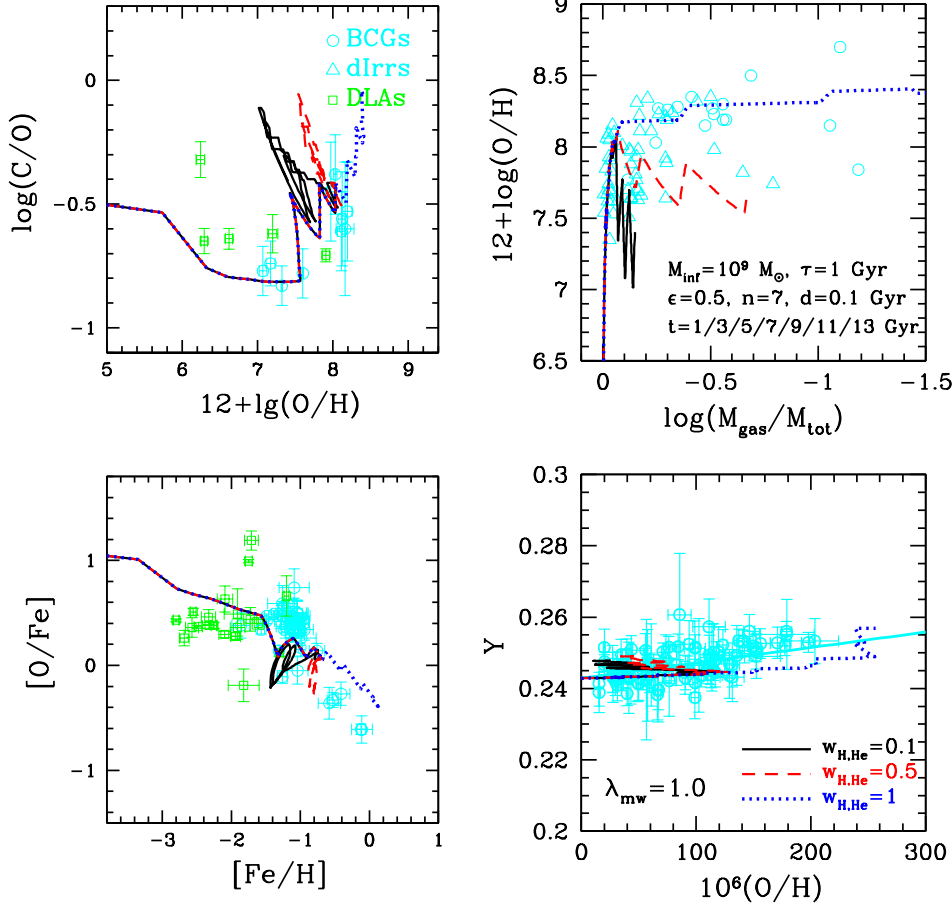


**Fig. 10.** The evolutionary track as predicted by models with various amounts of metal enhancements. The left two panels are  $\log(C/O)$  vs.  $12+\log(O/H)$  and  $[O/Fe]$  vs.  $[Fe/H]$ ; the right two panels are oxygen abundance vs. gas fraction and  $Y$  vs.  $(O/H)$ . All the 3 models have same bursts sequence ( $t = 1/3/5/7/9/11/13$  Gyr, and  $d = 0.1$  Gyr for each burst), but different degrees of metal enhancement. The *black-solid lines*, *red-dash lines*, *blue-dot lines* represent  $w_{\text{H,He}} = 0.1, 0.5, 1$  respectively. All these models assume the same total infall mass  $M_{\text{inf}} = 10^9 M_{\odot}$ . The observational data are the same as in Fig. 2, Fig. 3 and Fig. 4, BCGs, dIrrs, and DLAs are plotted in *cyan open circles*, *cyan open triangles* and *green open squares* here.

Since we assume a linear correlation between star formation rate and gas, the models with different total infalling masses are self-similar. Therefore, when the abundance ratios and gas fraction are examined (Figs. 5 and 6), the three series of models (M8, M9, and M10) are overlapping.

In Fig. 7 we plot the mass-metallicity relations predicted by models without wind. We run models for three different infall masses ( $10^8$ ,  $10^9$ ,  $10^{10} M_{\odot}$ ). The effects of different numbers of bursts ( $n = 1, 3, 7$ ), different durations ( $d = 0.03, 0.1, 0.3$ ) and different SFEs ( $\epsilon = 0.2, 0.5, 1.0, 2.0$ ) as functions of galactic mass are shown. It is evident from Fig. 7 that our models can very well reproduce the M-Z relation even without galactic wind but just assuming an increase of the number, or duration of bursts, or the efficiency of SF.

#### 4.2. Model with normal wind

If the galactic wind has the same chemical composition as the well-mixed ISM, i.e.  $w_i = 1$  for all the elements, we call it “normal wind”.

In Fig. 8, we show the the evolutionary tracks predicted by models with normal wind; abundance ratios of  $\log(C/O)$  vs.  $12+\log(O/H)$  and  $[O/Fe]$  vs.  $[Fe/H]$  are on the left side, while  $\mu - Z$  and  $Y - Z$  relations on the right side. The models have the same total infall mass ( $M_{\text{inf}} = 10^9 M_{\odot}$ ) and same bursts sequence ( $t = 1/3/5/7/9/11/13$  Gyr, with  $d = 0.1$  Gyr for each burst), but different wind efficiencies ( $\lambda_w = 0, 0.2, 0.5, 1.0$ ). Oxygen is produced by massive stars, therefore no oxygen will be ejected into the ISM after star formation ceases. On the other hand, elements, such as C and N produced by low- and intermediate-mass stars, and Fe mainly produced by SN Ia explosion, are continuously polluting the ISM after the star formation stops, owing to their long lifetime. Therefore, the decrease of the mass of gas (i.e., H and He) and the  $\alpha$ -elements lost with the wind will result in a dramatic increasing of the abundance of

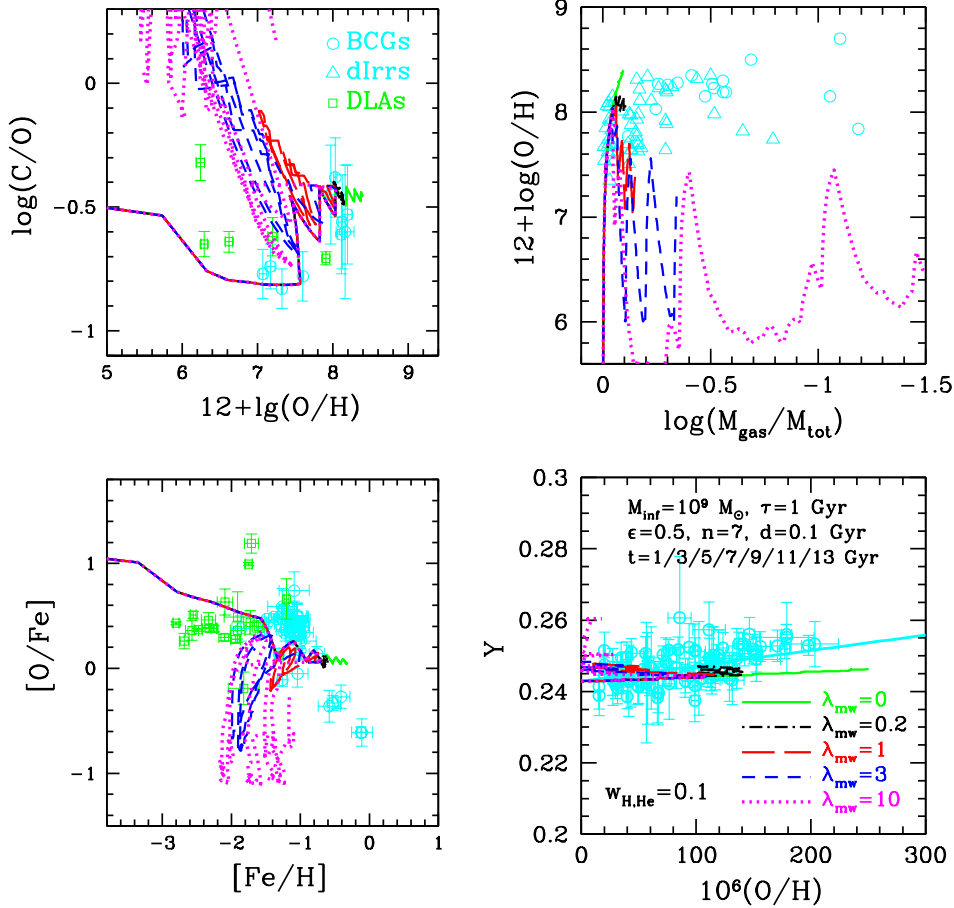


**Fig. 11.** The evolutionary track as predicted by models with various metal-enhanced wind efficiencies. The left two panels are  $\log(C/O)$  vs.  $12+\log(O/H)$  and  $[O/Fe]$  vs.  $[Fe/H]$ ; the right two panels are oxygen abundance vs. gas fraction and  $Y$  vs.  $(O/H)$ . All the 5 models have same bursts sequence ( $t = 1/3/5/7/9/11/13$  Gyr, and  $d = 0.1$  Gyr for each burst), but different wind efficiencies. *Green-solid lines*:  $\lambda_{mw} = 0$ ; *black-dash-dot lines*:  $\lambda_{mw} = 0.2$ ; *red-long-dash lines*:  $\lambda_{mw} = 1$ ; *blue-short-dash lines*:  $\lambda_{mw} = 3$ ; *magenta-dot lines*:  $\lambda_{mw} = 10$ . All these models assume the same total infall mass  $M_{\text{inf}} = 10^9 M_{\odot}$ . The observational data are the same as in Fig. 2, Fig. 3 and Fig. 4, BCDs, dIrrs, and DLAs are plotted in *cyan open circles*, *cyan open triangles* and *green open squares* here.

the “time-delayed” elements. The stronger the wind, the higher the abundance of C or Fe relative to O predicted by the models.

The main effect of normal winds is to decrease the gas fraction with a smaller effect on the O/H abundance, as we can see from the  $12+\log(O/H)-\mu$  relation (upper right panel of Fig. 8). This means that models with normal wind cannot explain the whole spread in O/H observed at a given  $\mu$  for these galaxies. There are two possible reasons for that. One is the same wind efficiency (i.e.,  $w_i \lambda_w$ ) for both oxygen and hydrogen in the normal wind, so that both O and H decrease at the same time. The other one is the short infall time scale assumed ( $\tau = 1$  Gyr). In this case, no primordial gas falls into the galaxies to dilute the ISM at late evolutionary times. Therefore, we also developed a model with long infall time scale ( $\tau = 10$  Gyr, magenta dotted lines in Fig. 8). It is clear that in this model the metallicity decreases in the interburst time. Actually, the infall of primordial gas (i.e., H and He) results in a lower mass loss rate of H and He than metals, similar to the metal-

enhanced wind case which will be further discussed in the next section. A very strong normal wind (e.g.  $\lambda_w > 0.5$ ) seems unlikely in late-type dwarf galaxies since it would lose a large amount of gas, and hence it would predict a too low gas fraction, as it is evident in Fig. 8. In the lower right panel of Fig. 8, the predicted  $Y$  vs.  $(O/H)$  relation is shown and it is consistent with the observational data at the low metallicity, because the wind does not develop yet when the galaxy is still very metal poor. However, after the wind, an increase of the helium abundance as well as of the abundances of elements produced on long timescale occurs, especially in the case of a strong wind which produces a very small final gas fraction.

In the last section, we have pointed out that the observed  $M - Z$  relation could indicate more star bursts or longer duration of each burst or higher SFE in more massive galaxies, if no outflow takes place. Now we examine the possibility of the normal wind being the explanation of the  $M - Z$  relation, as suggested by many previous authors. In Fig. 9, we take the models with 7 bursts

for example (i.e., Model M8n4, M9n4, M10n4 in no-wind case) but different strengths of normal wind are introduced ( $\lambda_w = 0, 0.2, 0.5, 1, 3$ ). It is evident from the upper panel of Fig. 9 that by varying only the efficiency of a normal wind one cannot reproduce the  $M - Z$  relation, unless other parameters, such as the efficiency of SF or the number of bursts, are assumed to vary as functions of the galactic mass. When a long infall timescale is adopted ( $\tau = 10$  Gyr, lower panel of Fig. 9), less stars are formed in each model due to the slow gas accretion process, and the wind could not be induced in the high mass systems ( $M_{inf} \approx 10^{10} M_\odot$ ). However in the low mass galaxy ( $M_{inf} = 10^8 M_\odot$ ), where the wind could develop, the newly infalling gas dilutes the ISM effectively. Therefore, the general trend of the  $M - Z$  relation could be reproduced by combining the normal wind with a slow accretion process.

In summary, the normal wind can strongly reduce the gas fraction but it cannot reduce sensibly the O/H. To explain the spread observed in O/H at the same  $\mu$  we should invoke other mechanisms, such as a continuous supplement of primordial gas or a metal-enhanced wind (see Sect. 4.3), both of which imply a lower mass loss rate for H and He relative to metals.

#### 4.3. Model with metal-enhanced wind

The galactic wind, mainly induced by SN explosion, could blow preferentially the metal-enriched gas out of the galaxy, which means metals are lost more efficiently than the gas (H and He). We define the wind “metal-enhanced” when the abundances of metals it carries out are higher than in the ISM. Metal-enhanced winds have been already suggested by several dynamical works (e.g. Mac Low & Ferrara 1999; Recchi et al. 2001, 2002). In our models we simply assume a higher wind efficiency weight  $w_i$  for heavy elements than H and He. In particular, we adopt  $w_i = 1 (i \neq \text{H, He})$ ,  $w_{\text{H,He}} < 1$ .

The wind models with various amounts of metal enhancements are shown in Fig. 10. All the models have same input parameters ( $\epsilon = 0.5$ , 7 bursts and the duration is 0.1 Gyr for each one) except for  $w_{\text{H,He}}$ . The model experiencing a highly enriched wind ( $w_{\text{H,He}} = 0.1$ ) loses very little gas. We show also models with mild metal-enhanced wind ( $w_{\text{H,He}} = 0.5$ ) and normal wind ( $w_{\text{H,He}} = w_{\text{O}} = 1$ ). The evolutionary tracks for the abundance ratios show a loop if the wind is metal-enriched. When the wind starts, oxygen is lost more efficiently than hydrogen, hence the oxygen abundance within the galaxy decreases with time in the interburst phase, and elements such as C and Fe will show increasing abundances relative to oxygen owing to their delayed restoration into the ISM. This trend continues until the new burst occurs. Because of the newly produced oxygen supplied to the ISM the O abundance increases and, as a consequence, the abundances of other elements relative to oxygen decrease. Therefore, the evolutionary track shows a loop. The lower the  $w_{\text{H,He}}$ , the more the metals lost, the lower the value that the O abundance reaches.

The metal-enhanced wind has also a dramatic influence on the  $\mu - Z$  relation, as we shown in the upper right panel of Fig. 10. The normal wind mainly reduces the gas fraction rather than the abundance, whereas the metal-enhanced wind is very powerful in reducing the metallicity of the galaxy.

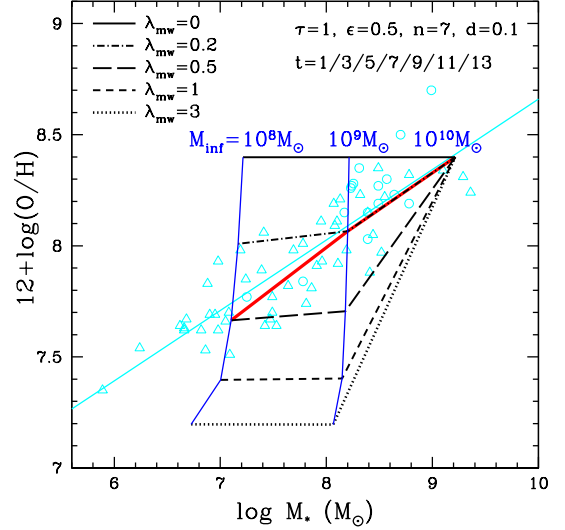


**Fig. 12.** Present day oxygen abundance vs.  $M_*$  as predicted by models with metal-enhanced wind ( $w_{\text{H,He}} = 0.1$ ). All the models contain 7 bursts and the same star formation history ( $\epsilon = 0.2, n = 7, t = 1/3/5/7/9/11/13, d = 0.1$  for each burst), and the total infall mass varies from  $M_{inf} = 10^8$  to  $10^{10} M_\odot$ . The predicted  $M - Z$  relation with different strength of metal-enhanced wind are shown in different lines: *black dash-dot, long-dash, short-dash, and dotted lines* are for  $\lambda_{mw} = 0, 0.2, 1, 3$  respective. Models with same  $M_{inf}$  are connected by *blue lines*. An increasing wind efficiency to less massive galaxies is shown in *red-solid line* which can fit the data very well. Observational data are shown in *cyan open circles* (BCDs) and *cyan open triangles* (dIrrs), the *cyan solid line* is the best fit of all data, same as in Fig. 1.

In Fig. 11, models with different strengths ( $\lambda_{mw} = 0, 0.2, 1, 3, 10$ ) of highly enriched winds ( $w_{\text{H,He}} = 0.1$ ) are shown. We plot the evolutionary tracks of models with same bursting history as in Fig. 10. A stronger wind not only reduces the abundances and increases the ratio between the long recycling term elements and the short ones, but also decreases the gas fraction dramatically. It is worth to point out that although the wind efficiencies  $\lambda_{mw}$  adopted here are much higher than the ones of normal wind case  $\lambda_w$ , the gas is lost less effectively. To compare the results of normal and metal-enhanced wind models, one should assume a larger  $\lambda_{mw}$  for the latter case. For example,  $\lambda_{mw} = 10$  for metal-enhanced winds is then multiplied by  $w_{\text{H,He}} = 0.1$ , therefore it is comparable with the case normal wind and  $\lambda_w = 1$ .

In the lower right panels of both Fig. 10 and Fig. 11 we show the  $Y - (\text{O}/\text{H})$  relations of galaxies with different degrees of enriched winds  $w_{\text{H,He}}$  and different wind efficiencies  $\lambda_{mw}$ , but the same formation histories. By comparing with Fig. 8, the present-day oxygen abundances are lower as we expect. In this scenario, a very high helium abundance can be reached at low metallicity level, especially when the wind is very strong, because most of it stays inside the galaxy while heavy elements are lost. The present-day  $Y - (\text{O}/\text{H})$  relation predicted by these models do not stay on a straight line in the low metallicity region, even if the unre-

**Table 3.** Parameters of the best models ( $w_{\text{H,He}} = 0.3$ ).

Model name			$\lambda_{mw}$	SFE	$n$	$t^1$	$d^2$ (Gyr)		
$10^8 M_\odot$	$10^9 M_\odot$	$10^{10} M_\odot$	$\text{Gyr}^{-1}$	$\text{Gyr}^{-1}$		Gyr	$10^8 M_\odot$	$10^9 M_\odot$	$10^{10} M_\odot$
M8b1	M9b1	M10b1	0.8	0.5	3	3/9/13	0.1*3	0.3*3	0.9*3
M8b2	M9b2	M10b2	0.8	0.5	5	1/3/7/10/13	0.1*5	0.3*5	0.9*5
M8b3	M9b3	M10b3	0.8	0.5	7	1/3/5/7/9/11/13	0.1*7	0.3*6	0.9*7
M8b4	M9b4	M10b4	0.8	0.5	9	1/2.5/4/5.5/7/8.5/10/11.5/13	0.1*9	0.3*9	0.9*9
DLA1			0.8	0.5	5	1/3/7/10/13	0.01/0.2*4		
DLA2			0.8	0.5	5	1/3/7/10/13	0.02/0.2*4		
DLA3			0.8	0.5	5	1/3/7/10/13	0.05/0.2*4		
DLA4			0.8	0.5	5	1/3/7/10/13	0.1/0.2*4		

Notes. <sup>(1)</sup> The middle time of the burst

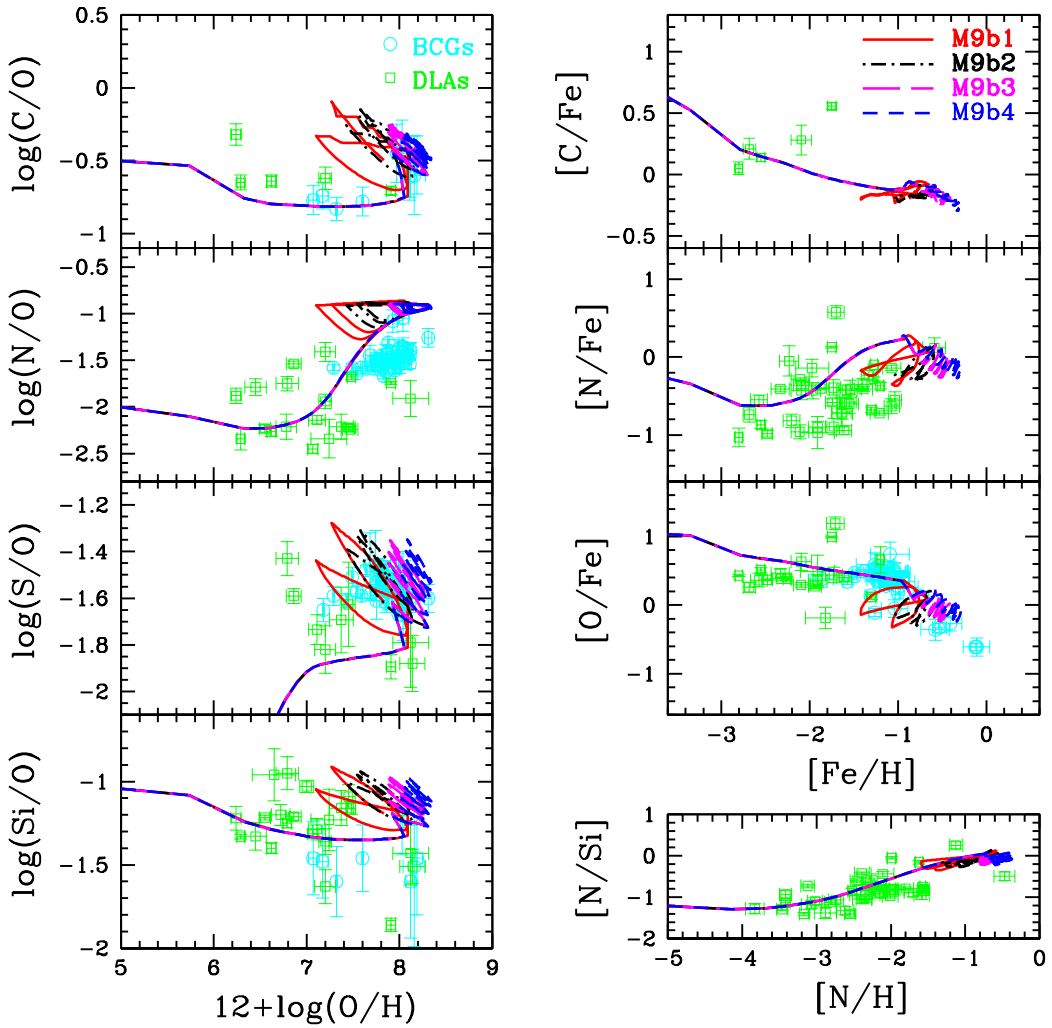


**Fig. 13.** The evolutionary track of abundance ratios of C/O, N/O, S/O, Si/O, C/Fe, N/Fe, O/Fe, and N/Si as predicted by our best models ( $M_{inf} = 10^9 M_\odot$ ) with metal-enhanced wind ( $w_{\text{H,He}} = 0.3$ ). The red-solid, black-dash-dot, magenta-long-dash and blue-short-dash lines are the results of M9b1, M9b2, M9b3 and M9b4 in Table. 3. The observational data are same as in Fig. 3, cyan open circles for BCDs and green open squares for DLAs.

alistic models (very strong wind  $\lambda_{mw} = 10$  cases) are ruled out considering their disagreement with other observational

constraints. Therefore, the observed scatter of  $Y-(\text{O}/\text{H})$  relation may be caused by metal-enhanced winds. Based on

**Table 4.** The maximum and present-day values of the SN Ia rates by number as predicted by the best models.

Model name	number of burst	$r_{\text{SN Ia}}(\text{century}^{-1})$	
		maximum	present day
M9b1	3	0.0218	0.0016
M9b2	5	0.0229	0.0012
M9b3	7	0.0229	0.0015
M9b4	9	0.0237	0.0016

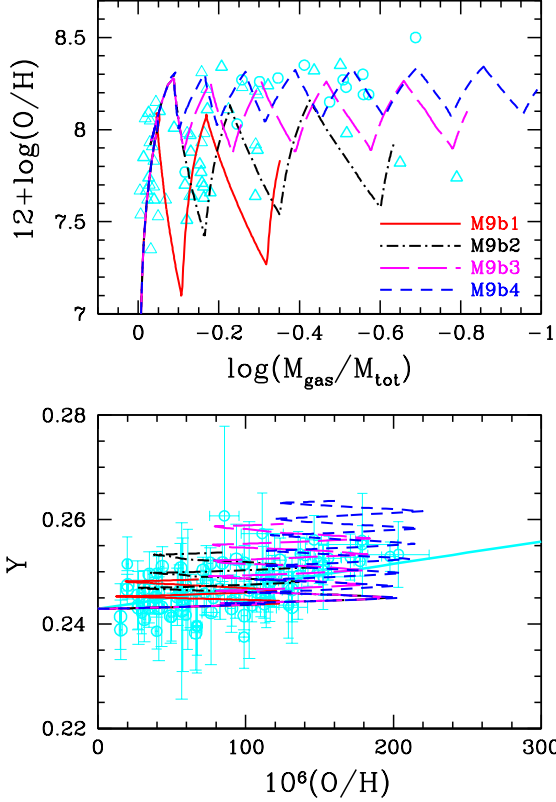


**Fig. 14.** The evolutionary tracks of  $12 + \log(\text{O}/\text{H})$  vs. gas fraction (*upper panel*) and  $Y - (\text{O}/\text{H})$  relation (*lower panel*) as predicted by our best models ( $M_{\text{inf}} = 10^9 M_{\odot}$ ) with metal-enhanced wind ( $w_{\text{H,He}} = 0.3$ ). The *red-solid*, *black-dash-dot*, *magenta-long-dash* and *blue-short-dash* lines are the results of M9b1, M9b2, M9b3 and M9b4 in Table. 3. The observational data are same as in Fig. 2 and Fig. 4, *cyan open circles* for BCDs and *cyan open triangles* for dIrrs.

our model predictions, we suggest to fit the lower envelop of the observational data, when one derives the primordial helium  $Y_p$ , because it may not be affected by the wind, hence the extrapolation to  $Z = 0$  will be more close to the real  $Y_p$ .

Fig. 12 is the same as Fig. 9 but for models with metal-enhanced wind. Unlike in the normal wind case, the metal-enhanced one is very effective in reducing the oxygen abundance, hence in creating the  $M - Z$  relation. The stronger the wind efficiency, the steeper the predicted  $M - Z$ . Therefore, models with an increasing wind efficiency to less massive galaxies are consistent with the observations very well. As a conclusion, the observed  $M - Z$  re-

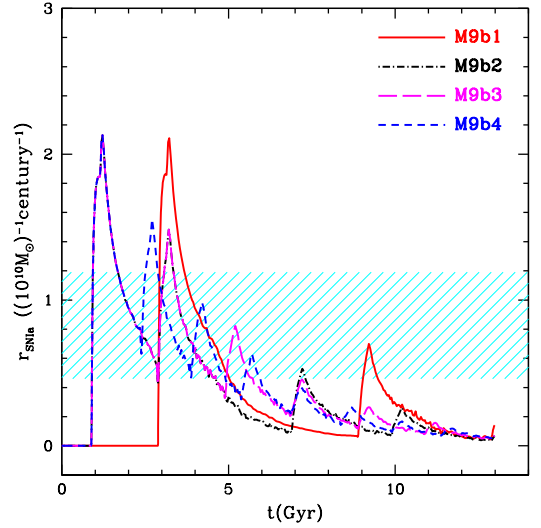


**Fig. 15.** The SN Ia rate normalized to the galaxy stellar mass as a function of time as predicted by our best models ( $M_{\text{inf}} = 10^9 M_{\odot}$ ). The *red-solid*, *black-dash-dot*, *magenta-long-dash* and *blue-short-dash* lines are for model M9b1, M9b2, M9b3 and M9b4 respectively. As a comparison, the *shaded area* shows the observed range of normalized SN Ia rate in the Irr galaxies,  $0.77^{+0.42}_{-0.31}$  per century and per  $10^{10} M_{\odot}$  (Mannucci et al. 2005).

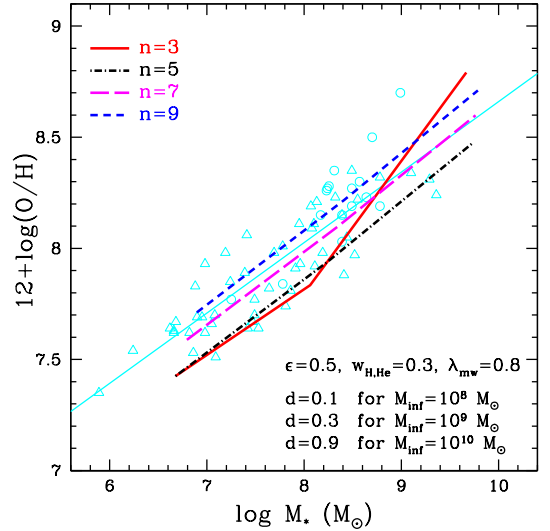


**Fig. 16.** The mass-metallicity relation as predicted by our best models. The total infalling masses range from  $M_{\text{inf}} = 10^8$  to  $10^{10} M_{\odot}$ , and more massive one prefers longer duration of burst. The results with different numbers of burst are shown in different lines, *red-solid*, *black-dash-dot*, *magenta-long-dash* and *blue-short-dash* lines are for  $n = 3, 5, 7, 9$  respectively. The observational data of BCDs (*cyan open circles*) and dIrrs (*cyan open triangles*) are the same as in Fig. 1.

lation could be caused by metal-enhanced winds with mild strength (e.g.,  $\lambda_{\text{mw}} \leq 1$ ).

In summary, metal-enhanced winds should take place in late-type dwarf galaxies, and they play an important role in removing gas, especially the metals, out of the galaxies.

#### 4.4. Best models

As we have shown in the last section, highly enriched or very strong winds will reduce the galactic oxygen abundance to a very low value during the interburst time which has not been confirmed from the observational point of view. Thus, in our best models  $w_{\text{H,He}} = 0.3$  and  $\lambda_{mw} = 0.8$  are assumed. Different numbers of bursts are examined for  $M_{inf} = 10^9 M_{\odot}$  galaxies, and the best fit models are shown in Fig. 13 and Fig. 14. In these models, the same SFEs ( $\epsilon = 0.5$ ) and burst durations ( $d=0.3$ ) are assumed, and the details of each model are listed in Table. 3.

We show the abundance ratios of different elements relative to oxygen or iron as predicted by our best models for  $M_{inf} = 10^9 M_{\odot}$  in Fig. 13. The evolutionary tracks of these models can pass through the DLA data at early time, and cover the regions where most of BCDs have been observed.

The evolutionary tracks of the  $\mu - Z$  relation (upper panel) and  $Z - Y$  relation (lower panel) predicted by our best models are shown in Fig. 14. After the wind develops, more are the bursts that a galaxy suffers, more are the oscillations in the evolutionary tracks, and these tracks pass through most of the data, thus explaining the observed spread. On the other hand, in the panel showing  $Y$  vs.  $(\text{O}/\text{H})$  helium keeps increasing while O is oscillating and this is due to the fact that this element is produced also during the interburst periods and lost less effectively than O. This implies again that we should use the lower envelope of the observational data to derive the primordial abundance of helium.

In Fig. 15, we show the evolution of the Type Ia supernova rates predicted by our best models. The rates in this figure are normalized to the galaxy stellar mass at that time, i.e., expressed in number of SNe per century and per  $10^{10} M_{\odot}$ . The peaks are always associated with the star formation periods, but SNe Ia also explode during the interburst times. Compared to the observed value quoted for the Irr galaxies,  $0.77^{+0.42}_{-0.31}$  per century and per  $10^{10} M_{\odot}$  (Mannucci et al. 2005), our model predicts a very high normalized SN Ia rate during the first star formation burst, but  $\sim 1 - 2$  Gyr later, the rate decays, and becomes comparable to the Irr galaxies in the following SF periods. In these best models, the maximum of SN Ia rate by number varies between 0.022 and 0.024 per century and the present value varies between 0.0012 and 0.0016 per century (see Table 4). Sullivan et al. (2006) have studied the relation between SN Ia rate and the stellar mass of the host galaxy in the redshift range 0.2 – 0.75, and they found the SN Ia rate is less than 0.01 per century for star-forming galaxies whose stellar mass around  $10^8 M_{\odot}$ , in agreement with our predictions.

In order to reproduce the mass-metallicity relation, we have studied galaxies of different masses, with more massive galaxies preferring longer star formation bursts,  $d = 0.9$  Gyr for  $M_{inf} = 10^{10} M_{\odot}$  and  $d = 0.1$  Gyr for  $M_{inf} = 10^8 M_{\odot}$  (see details in Table 3). The mass-metallicity relations predicted by our best models with different numbers of bursts are shown in Fig. 16, and they are consistent with the observed one considering the scatter of the data, espe-

cially in the cases where the wind develops in the whole galactic mass range (i.e.,  $n \geq 5$ ).

Considering that dwarf galaxies could be in different evolutionary stages and/or have different ages (measured from the beginning of star formation), we show that our best models – a series of uniform models with same  $M_{inf}$ ,  $w_{\text{H,He}}$ ,  $\lambda_{mw}$ ,  $\epsilon$ ,  $d$  but different  $n$  and suitable  $t$  – can well reproduce the spread in the observations. *Therefore, our preferred galaxy formation scenario for these galaxies is the following: they should have accreted a lot of primordial gas at their early stages, and formed stars through several short star bursts ( $d \sim 0.3$  Gyr for  $M_{inf} = 10^9 M_{\odot}$ ), with more massive galaxies suffering longer star formation bursts. However, it is likely that the gas escape from the potential well of the galaxy when enough energy from SN explosions is accumulated, and this wind should be metal-enhanced ( $w_{\text{H,He}} \sim 0.3$ ). The wind rate should be proportional to the gas mass at that time, and the wind efficiency should be  $\lambda_{mw} < 1$ .*

DLAs could be the progenitors of dwarf irregular galaxies, as already suggested by Matteucci et al. (1997) and Calura et al. (2003). In our best models, we adopted a fixed duration for each burst with the purpose of changing the parameters as less as possible. The evolutionary tracks of our best models pass through the DLA data, but could not explain the scatter. However, if we reduce the duration of the first SF burst to  $d = 0.01 \sim 0.1$  Gyr, by taking model M9b3 as an example, the models can explain the scatter in the abundance ratios of DLAs much better (see Fig. 17 and Table 3 for details of these models). Therefore, we confirm that the DLA systems could be progenitors of local dwarf galaxies.

#### 4.5. Continuous star formation

By using a spectrophotometric model coupled with a chemical evolution model, Legrand (2000) demonstrated that a continuous but very mild star formation rate (SFE as low as  $10^{-3} M_{\odot} \text{Gyr}^{-1}$ ) is able to reproduce the main properties of IZw 18, one of the most metal-poor BCDs we know. Therefore, in this section we are showing model results obtained with continuous and mild SF.

We run the same models as in Legrand (2000), one model with a mild continuous SF ( $\epsilon = 0.001 \text{Gyr}^{-1}$ ) only, and the other one with a mild continuous SF ( $\epsilon = 0.001 \text{Gyr}^{-1}$ ) and a current burst ( $SFR = 0.023 M_{\odot} \text{yr}^{-1}$ , i.e.,  $\epsilon = 0.88 \text{Gyr}^{-1}$  if the observed  $M_{\text{HI}} = 2.6 \times 10^7 M_{\odot}$ , during the last 20 Myrs). The abundance ratios of different elements as predicted by these two models are shown in Fig. 18. As expected, such a low continuous SF predicts a too low oxygen abundance which could not explain the majority of local BCDs. In addition, by examining the evolutionary tracks in the low metallicity range, one sees that DLAs cannot be the progenitors of such galaxies.

Therefore, we developed other models with higher SFEs and different SF duration. Since both dIrrs and BCDs harbor recent SF activities, we assumed that the SF is still going on at the present day, and therefore a short duration  $d$  implies a late starting time ( $t_G - d$ ) of SF.

We have examined the models with different SFHs by varying the SFE, duration, and infall timescale. The results show that only models with different SFEs are able to explain the scatters in the abundance ratios. In Fig. 19,

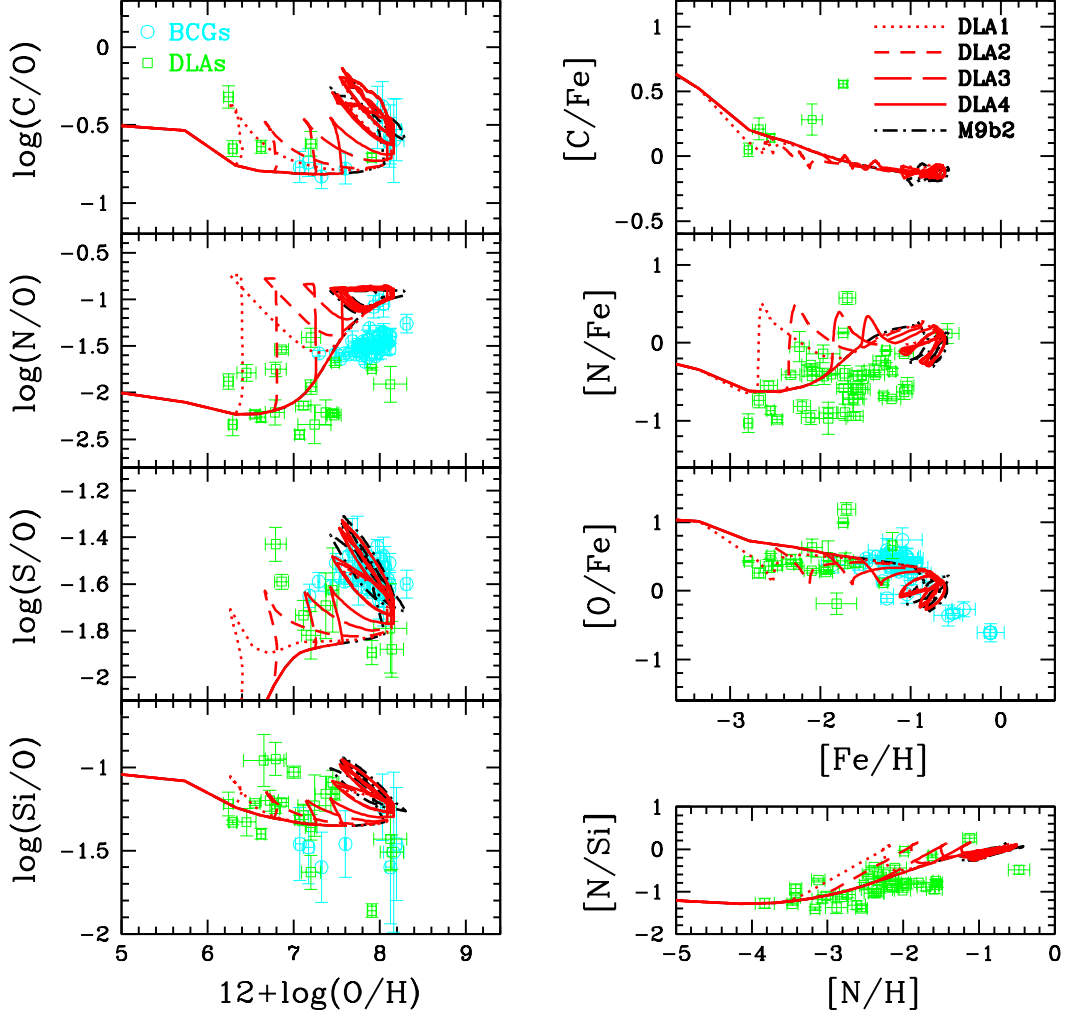


**Fig. 17.** The evolutionary track of abundance ratios as predicted by our DLA models. All of these models assume same SFHs as model M9b3 except for a shorter duration of the first burst used. The red *dotted*, *short-dash*, *long-dash* and *solid* lines are for models DLA1 to DLA4 whose durations of the first burst are  $d = 0.01, 0.02, 0.05, 0.1$  Gyr respectively. As a comparison, we also show the best model M9b2 of dwarf galaxy in black-dash-dot lines. All these models assume the same total infall mass  $M_{inf} = 10^9 M_{\odot}$ . Cyan open circles are BCDs and green open squares are DLAs, same as in Fig. 3.

models with different SFEs for the cases of no wind (left column), normal wind (middle column), and metal-enhanced wind ( $w_{\text{H,He}} = 0.3$ , right column) are shown. In these models, to avoid reaching a too high metallicity at the present time, a duration shorter than the age of the universe is assumed for the highest SFE case. A short infall timescale is adopted ( $\tau = 1$  Gyr) here, because it does not effect the evolutionary track too much in the continuous SF scenario, especially when the SF starts late.

There are several conclusions that can be drawn from Fig. 19:

1. In the case of no wind, although models with different  $\epsilon$  could partly explain the scatters in the abundance ratios, they cannot reproduce the  $\mu - Z$  relation. As we can see from the bottom left panel of Fig. 19, all the evolutionary tracks are overlapping, the same as in the bursting SF scenario without galactic wind;
2. When the wind is included in the model, the gas fraction decreases with time (the bottom middle and right panels of Fig. 19). We adopt relatively high wind efficiencies in the continuous SF scenario. When we compare the models with the same SFE in both normal wind and metal-enhanced wind cases, we can see that their gas fractions reach almost the same values at the present time since their gas loss rates are comparable ( $\lambda_w = w_{\text{H,He}} \lambda_{mw} = 0.6$ ); however, their metals show different behaviors. The oxygen abundance decreases dramatically in the metal-enhanced wind case, thus explaining the scatter in  $\mu - Z$  relation much better. In the meantime, the metal enhanced wind model can fit the data relative to abundance ratios much better (upper and middle panels of right column in Fig. 19);
3. As we have demonstrated before, galaxies with long continuous but mild SF (e.g.,  $\epsilon = 0.01$ ,  $d = 13$ ), which could be the case for some BCDs, as suggested by

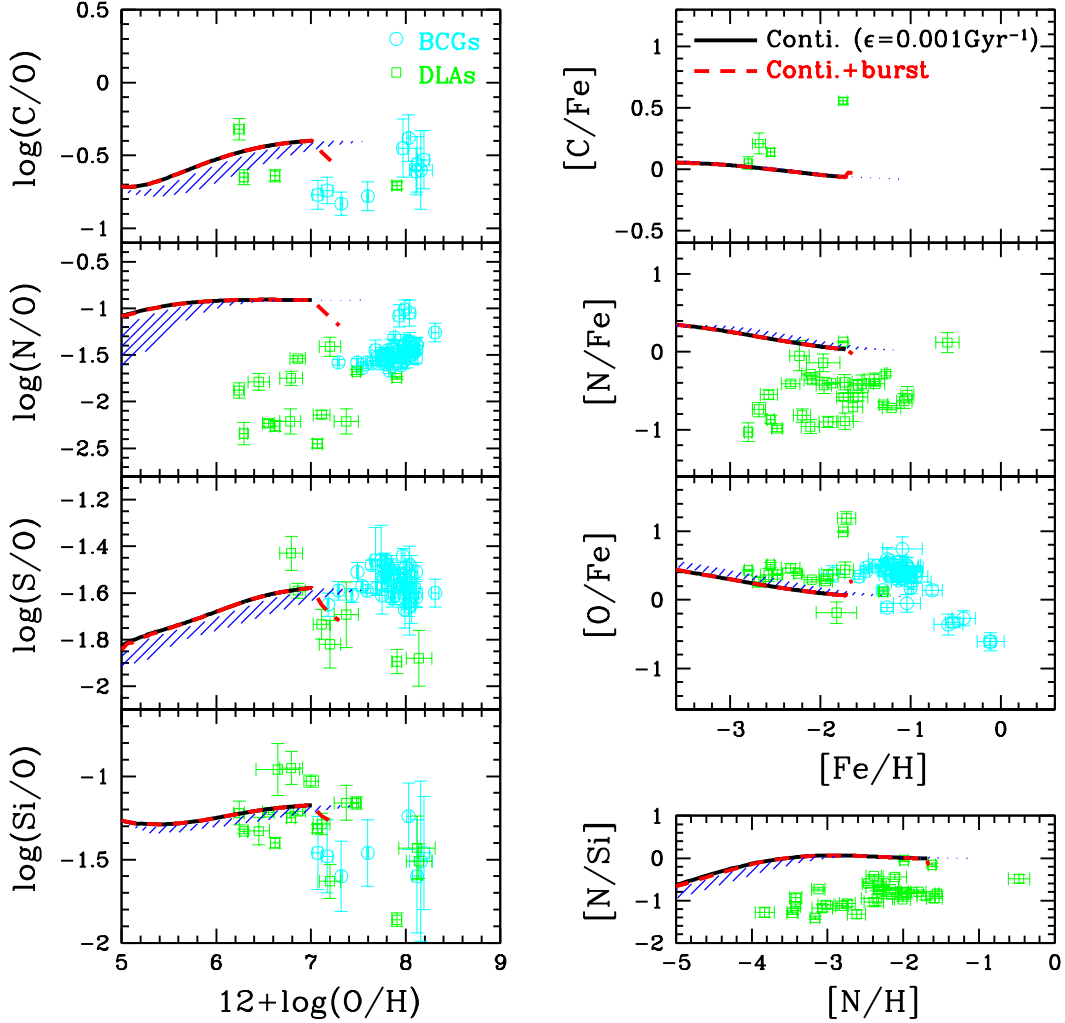


**Fig. 18.** The evolutionary track of abundance ratios as predicted by the models of Legrand (2000). A mild continuous SF with  $\epsilon = 0.001 \text{ Gyr}^{-1}$  is shown in *black-solid lines*, whereas a mild continuous SF ( $\epsilon = 0.001 \text{ Gyr}^{-1}$ ) combined with a current burst ( $SFR = 0.023 M_{\odot} \text{ yr}^{-1}$ , i.e.,  $\epsilon = 0.88 \text{ Gyr}^{-1}$  if  $M_{\text{HI}} = 2.6 \times 10^7 M_{\odot}$ , during the last 20 Myrs) is shown in *red-dash lines*. The *blue shade areas* show the continuous SF with  $1.45 \times 10^{-3} \leq \epsilon \leq 3.85 \times 10^{-3} \text{ Gyr}^{-1}$  which is derived from the observed SFR and  $M_{\text{HI}}$  data of IZw 18 (see Table 1 of Legrand 2000). *Cyan open circles* are BCDs and *green open squares* are DLAs, same as in Fig. 3.

the previous work (e.g., Legrand 2000; Legrand et al. 2000), should not be the majority due to the too low predicted oxygen abundances. Their evolutionary tracks relative to abundance ratios also do not fit the data. In addition, DLAs cannot be the progenitors of these objects when abundance ratios are examined, because of the very high predicted values of N/O, N/Fe and N/Si at low metallicity (see Fig. 18), at variance with the properties of DLAs.

- In the continuous SF scenario, the optimal models should have  $\epsilon = 0.05 - 0.2$ , a duration of SF shorter than 13 Gyr, and metal-enhanced winds should occur, a situation similar to a long starburst scenario. Moreover, DLAs can be the progenitors of these galaxies.

## 5. Discussion and Conclusions

We have discussed in detail the chemical evolution of late-type dwarf galaxies (dwarf irregular and blue compact galaxies) and used the most recent data as a comparison. We have taken into account the measured abundances of single elements (He, C, N, O, S, Si and Fe) as well as the gas masses. We have assumed that the late-type dwarf galaxies form by cold gas accretion and we run models for different accreted baryonic masses ( $10^8, 10^9$  and  $10^{10} M_{\odot}$ ). We have tested both bursting and continuous star formation. We then have studied in detail the development of galactic winds by assuming a dark matter halo which is assumed 10 times the amount of the baryonic mass and feedback from SNe and stellar winds. Our main conclusions are:

- Galactic winds are necessary to reproduce the main properties of late-type dwarf galaxies and they should

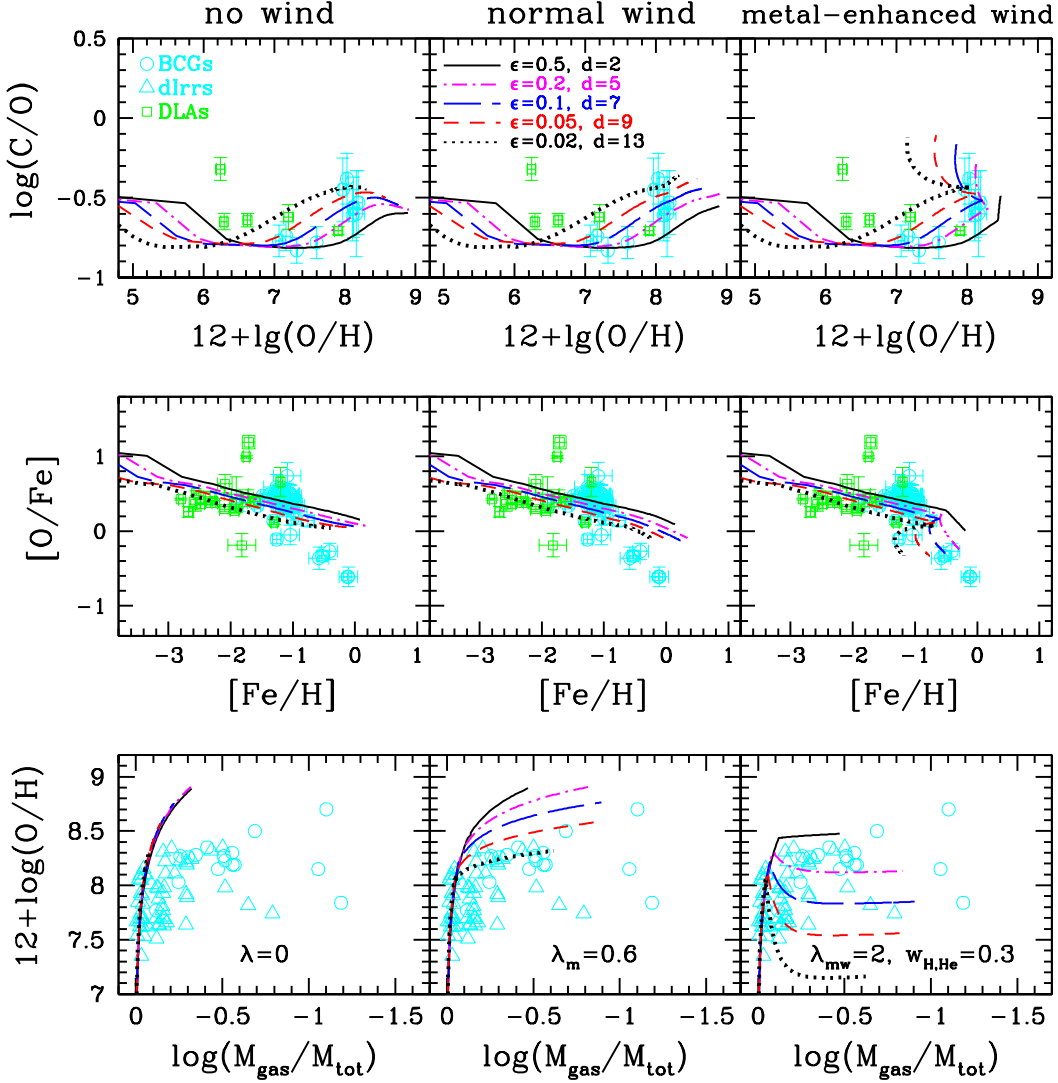


**Fig. 19.** The evolutionary track as predicted by models with continuous star formation. From top to bottom panels are  $\log(\text{C}/\text{O})$  vs.  $12+\log(\text{O}/\text{H})$ ,  $[\text{O}/\text{Fe}]$  vs.  $[\text{Fe}/\text{H}]$ , and the  $mu - Z$  relation; from left to right columns are for the cases of no wind, normal wind, and metal-enhanced wind ( $w_{\text{H,He}} = 0.3$ ). Models with different SFEs are shown in each case: *black-solid lines* for  $\epsilon = 0.5$  ( $d = 2$ ), *magenta-dash-dot lines* for  $\epsilon = 0.2$  ( $d = 5$ ), *blue-long-dash lines* for  $\epsilon = 0.1$  ( $d = 7$ ), *red-dash lines* for  $\epsilon = 0.05$  ( $d = 9$ ), and *black-dot lines* for  $\epsilon = 0.02$  ( $d = 13$ ). The total infall masses are assumed to be  $M_{\text{inf}} = 10^9 M_{\odot}$  in all these models. The observational data are the same as in Fig. 2 and Fig. 3, BCDs, dIrrs, and DLAs are plotted in *cyan open circles*, *cyan open triangles* and *green open squares* respectively.

be metal-enhanced, namely metals should be carried away preferentially, in agreement with previous dynamical work (e.g. Mac Low & Ferrara 1999; Recchi et al. 2001). The rate of gas loss was assumed to be proportional to the amount of gas present at the time of the wind, which is equivalent to say that is proportional to the SFR, in agreement with previous papers and observational evidence (Martin 2005; Rupke et al. 2005; Chen et al. 2010). The wind efficiency  $\lambda_{mw}$  should be relatively low ( $\lambda_{mw} \sim 0.8$  in bursting SF scenario, and  $\lambda_{mw} \sim 2$  in continuous SF scenario) compared to what is assumed for dwarf spheroidals ( $\sim 6$  to 15) where the wind should carry away all the residual gas (e.g. Lanfranchi & Matteucci 2003).

2. Both bursting and continuous SF scenarios have been examined. In the case of bursting SF, the number of

bursts could be no more than  $\sim 10$  and the star formation efficiency could be  $\sim 0.5 \text{ Gyr}^{-1}$ . Galaxies with a long continuous but mild SF ( $\epsilon \lesssim 0.02 \text{ Gyr}^{-1}$ ,  $d \simeq 13 \text{ Gyr}$ ) should not be the majority, whereas galaxies with higher SFE ( $0.05 \text{ Gyr}^{-1} \lesssim \epsilon \lesssim 0.2 \text{ Gyr}^{-1}$ ) and shorter SF duration ( $5 \text{ Gyr} \lesssim d \lesssim 9 \text{ Gyr}$ ) are still acceptable.

3. Models with a different number of bursts and/or different star formation efficiency and/or different burst duration, coupled with metal enhanced winds, can reproduce at best the spread observed in the abundances versus fractionary mass of gas and abundance ratios versus abundances. Normal winds, where all the gas and metals are lost at the same rate, should be rejected since they subtract too much gas.

4. We studied the  $M - Z$  relation for late-type dwarf galaxies and we showed that in order to reproduce such a re-

lation one should assume that different galaxies suffered an increasing amount of star formation (efficiency, number of bursts, duration of bursts) with galactic mass, even without galactic winds. However, metal-enhanced wind are necessary to reproduce all the other features. In the case of the  $M - Z$  relation, a metal-enhanced wind efficiency increasing with galactic mass can very well reproduce the data, leaving all the other parameters to be the same irrespective of the galactic mass. On the other hand, normal winds occurring at a different efficiency in different galaxies cannot reproduce the  $M - Z$  relation unless the primordial gas is infalling continuously (i.e., a long infall timescale), or the SFE or the number of bursts increase with galactic mass.

5. A comparison of our best model predictions with data for DLAs has shown that these objects can well be the progenitors of local dIrrs and BCDs, in agreement with previous papers.
6. In this work, our models can reproduce the chemical properties of both dIrrs and BCDs. To distinguish between these two types of galaxies, the photometric and spectral information should also be taken into account.

**Acknowledgements.** J.Y. thanks the hospitality of the Department of Physics of the University of Trieste where this work was accomplished. J.Y. and F.M. acknowledge the financial support from PRIN2007 from Italian Ministry of Research, Prot. no. 2007JJC53X-001. J.Y. also thanks the financial support from the National Science Foundation of China No.10573028, the Key Project No.10833005, the Group Innovation Project No.10821302, 973 program No. 2007CB815402, and the Knowledge Innovation Program of the Chinese Academy of Sciences No. Y090761009. Finally, we thank the referee, Leticia Carigi, for carefully reading the manuscript and giving us very useful suggestions.

## References

- Abate, A., Bridle, S., Teodoro, L. F. A., Warren, M. S., & Hendry, M. 2008, *MNRAS*, 389, 1739
- Aloisi, A., Clementini, G., Tosi, M., Annibali, F., Contreras, R., Fiorentino, G., Mack, J., Marconi, M., et al. 2007, *ApJ*, 667, L151
- Bertin, G., Saglia, R. P., & Stiavelli, M. 1992, *ApJ*, 384, 423
- Bomans, D. J. Chu, Y.-H., & Hopp, U. 1997, *ApJ*, 113, 1678
- Bradamante F., Matteucci F., & D’Ercole A. 1998, *A&A*, 337, 338
- Brodie, J. P., & Huchra, J. P. 1991, *ApJ*, 379, 157
- Calura, F., Matteucci, F., & Vladilo, G. 2003, *MNRAS*, 340, 59
- Carigi, L., Colín, P., & Peimbert, M. 1999, *ApJ*, 514, 787
- Centurión, M., Molaro, P., Vladilo, G., Péroux, C., Levshakov, S. A., & D’Odorico, V. 2003, *A&A*, 403, 55
- Chen, Y. M., Tremonti, C. A., Heckman, T. M., Kauffmann, G., Weiner, B. J., Brinchmann, J., Wang, J. 2010, arXiv:1003.5425
- Dekel, A. & Silk, J. 1986, *ApJ*, 303, 39
- Dessauges-Zavadsky, M., Calura, F., Prochaska, J. X., D’Odorico, S., & Matteucci, F. 2004, *A&A*, 416, 79
- Dessauges-Zavadsky, M., Calura, F., Prochaska, J. X., D’Odorico, S., & Matteucci, F. 2007, *A&A*, 470, 431
- Dessauges-Zavadsky, M., D’Odorico, S., McMahon, R. G., Molaro, P., Ledoux, C., Péroux, C., Storrie-Lombardi, L. J. 2001, *A&A*, 370, 426
- Dessauges-Zavadsky, M., Prochaska, J. X., D’Odorico, S., Calura, F., & Matteucci, F. 2006, *A&A*, 445, 93
- De Young, D. S. & Gallagher, J. S. 1990, *ApJ*, 356, 15
- D’Odorico, V., & Molaro, P. 2004, *A&A*, 415, 879
- Ekta, B. & Chengalur, J. N. 2010, *MNRAS*, 406, 1238
- Ellison, S. L. & Lopez, S. 2001, *A&A*, 380, 117
- Ellison, S. L., Pettini, M., Steidel, C. C., & Shapley, A. E. 2001, *ApJ*, 549, 770
- Fujita, A., Martin, C. L., Mac Low, M.-M., & Abel, T. 2003, *ApJ*, 599, 50
- Ferrara, A. & Tolstoy E. 2000, *MNRAS*, 313, 291, 309
- Garnett, D. R. 2002, *ApJ*, 581, 1019
- Garnett, D. R. & Shields, G. A. 1987, *ApJ*, 317, 82
- Grebel, E. K. 2001, *ASPC*, 239, 280
- Guseva, N. G., Izotov, Y. I., Papaderos, P., Chaffee, F. H., Foltz, C. B., Green, R. F., Thuan, T. X., Fricke, K. J., & Noeske, K. G. 2001, *A&A*, 378, 756
- Guseva, N. G., Papaderos, P., Izotov, Y. I., Green, R. F., Fricke, K. J., Thuan, T. X., & Noeske, K. G. 2003a, *A&A*, 407, 91
- Guseva, N. G., Papaderos, P., Izotov, Y. I., Green, R. F., Fricke, K. J., Thuan, T. X., & Noeske, K. G. 2003b, *A&A*, 407, 105
- Henry, R. B. C., Edmunds, M. G., & Köppen, J. 2000, *ApJ*, 541, 660
- Henry, R. B. C. & Prochaska, J. X. 2007, *PASP*, 119, 962
- Izotov, Y. I., Chaffee, F. H., Foltz, C. B., Green, R. F., Guseva, N. G., & Thuan, T. X. 1999, *ApJ*, 527, 757
- Izotov, Y. I., Chaffee, F. H., & Green, R. F. 2001a, *ApJ*, 562, 727
- Izotov, Y. I., Chaffee, F. H., & Schaerer, D. 2001b, *A&A*, 378, L45
- Izotov, Y. I., Schaerer, D., Blecha, A., Royer, F., Guseva, N. G., & North, P. 2006, *A&A*, 459, 71
- Izotov, Y. I. & Thuan, T. X. 1998a, *ApJ*, 497, 227
- Izotov, Y. I. & Thuan, T. X. 1998b, *ApJ*, 500, 188
- Izotov, Y. I. & Thuan, T. X. 1999, *ApJ*, 511, 639
- Izotov, Y. I. & Thuan, T. X. 2004a, *ApJ*, 602, 200
- Izotov, Y. I. & Thuan, T. X. 2004b, *ApJ*, 616, 768
- Izotov, Y. I., Thuan, T. X., & Lipovetsky, V. A. 1997, *ApJS*, 108, 1
- Jenkins, E. B. 2009, *ApJ*, 700, 1299
- Karachentsev, I. D., Karachentseva, V. E., Huchtmeier, W. K., & Makarov, D. I. 2004, *AJ*, 127, 2031
- Kauffmann, G., White, S. D. M., & Guiderdoni, B. 1993, *MNRAS*, 264, 201
- Kulkarni, V. P., Huang, K., Green, R. F., Bechtold, J., Welty, D. E. & York, D. G. 1996, *MNRAS*, 279, 197
- Kunth, D., Maurogordato, S., & Vigroux, L. 1988, *A&A*, 204, 10
- Lamareille, F., Mouhcine, M., Contini, T., Lewis, I., & Maddox, S. 2004, *MNRAS*, 350, 396
- Lanfranchi G. A., & Matteucci F. 2003, *MNRAS*, 345, 71
- Larson, R. 1974, *MNRAS*, 169, 229
- Lee, H., McCall, M. L., Kingsburgh, R., Ross, R., & Stevenson, C. C. 2003a, *AJ*, 125, 146
- Lee, H., McCall, M. L., & Richer, M. G. 2003b, *AJ*, 125, 2975
- Lee, H., Skillman, E. D., Cannon, J. M., Jackson, D. C., Gehrz, R. D., Polonski, E. F., & Woodward, C. E. 2006, *ApJ*, 647, 970
- Lee, J. C., Salzer, J. J., & Melbourne, J. 2004, *ApJ*, 616, 752
- Ledoux, C., Petitjean, P., Fynbo, J. P. U., Møller, P., & Srianand, R. 2006, *A&A*, 457, 71
- Ledoux, C., Petitjean, P., & Srianand, R. 2003, *MNRAS*, 346, 209
- Legrand, F. 2000, *A&A*, 354, 504
- Legrand, F., Kunth, D., Roy, J.-R., Mas-Hesse, J. M., & Walsh, J. R. 2000, *A&A*, 355, 891
- Lequeux, J., Peimbert, M., Rayo, J. F., Serrano, A., & Torres-Peimbert, S. 1979, *A&A*, 80, 155
- Levshakov, S. A., Dessauges-Zavadsky, M., D’Odorico, S., Molaro, P. 2002, *ApJ*, 565, 696
- Lipovetsky, V. A., Chaffee, F. H., Izotov, Y. I., Foltz, C. B., Kniazev, A. Y., & Hopp, U. 1999, *ApJ*, 519, 177
- Lopez, S. & Ellison, S. L. 2003, *A&A*, 403, 573
- Lopez, S., Reimers, D., D’Odorico, S., & Prochaska, J. X. 2002, *A&A*, 385, 778.
- Lu, L., Sargent, W. L. W., Barlow, T. A., Churchill, C. W., & Vogt, S. S. 1996, *ApJS*, 107, 475
- Luridiana, V., Peimbert, A., Peimbert, M., & Cerviño, M. 2003, *ApJ*, 592, 846
- Mac Low, M.-M. & Ferrara, A. 1999, *ApJ*, 513, 142
- Mannucci F., Della valle M., Panagia N., Cappellaro E., Cresci G., Maiolino R., Petrosian A., & M. Turatto. 2005, *A&A*, 433, 807
- Marconi, G., Matteucci, F., & Tosi, M. 1994, *MNRAS*, 270, 35
- Martin, C. L. 1996, *ApJ*, 465, 680
- Martin, C. L. 2005, *ApJ*, 621, 227

- Martin, C. L., Kobulnicky, H. A., & Heckman T. M. 2002, *ApJ*, 574, 663
- Martín-Manjón, M. L., Mollá, M., Díaz, A. I., & Terlevich, R. 2008, *MNRAS*, 385, 854.
- Martín-Manjón, M. L., Mollá, M., Díaz, A. I., & Terlevich, R. 2009, arXiv0901.1186
- Mateo, M. 1998, *ARA&A*, 36, 435
- Matteucci, F. & Chiosi, C. 1983, *A&A*, 123, 121
- Matteucci, F., Molaro, P., & Vladilo, G. 1997, *A&A*, 321, 45
- Matteucci, F. & Tosi, M. 1985, *MNRAS*, 217, 391
- Mendes de Oliveira, C., Temporin, S., Cypriano, E. S., Plana, H., Amram, P., Sodr e, L., Jr., & Balkowski, C. 2006, *AJ*, 132, 570
- Meurer, G. R., Freeman, K. C., Dopita, M. A., & Cacciari C. 1992, *AJ*, 103, 60
- Molaro, P., Levshakov, S. A., D’Odorico, S., Bonifacio, P. & Centuri on, M. 2001, *ApJ*, 549, 90
- Noterdaeme, P., Petitjean, P., Ledoux, C., Srianand, R., & Ivanchik, A. 2008, *A&A*, 491, 397
- Noterdaeme, P., Petitjean, P., Srianand, R., Ledoux, C., & Le Petit, F. 2007, *A&A*, 469, 425
- O’Meara, J. M., Bures, S., Prochaska, J. X., Prochter, G. E., Bernstein, R. A., Burgess, K. M. 2006, *ApJ*, 649, L61
-  stlin, G. 2000, *ApJ*, 535, L99
- Outram, P. J., Chaffee, F. H., & Carswell, R. F. 1999, *MNRAS*, 310, 289
- Papaderos, P., Guseva, N. G., Izotov, Y. I., Noeske, K. G., Thuan, T. X., & Fricke, K. J. 2006, *A&A*, 457, 45
- Papaderos, P., Izotov, Y. I., Thuan, T. X., Noeske, K. G., Fricke, K. J., Guseva, N. G., & Green, R. F. 2002, *A&A*, 393, 461
- Papaderos, P., Loose, H.-H., Thuan, T. X., & Fricke, K. J. 1996, *A&AS*, 120, 207
- Peimbert, A. 2003, *ApJ*, 584, 735
- Peimbert, M., Luridiana V., & Peimbert A. 2007, *ApJ*, 666, 636
- P rez-Gonz lez, P. G., Gil de Paz, A., Zamorano, J., Gallego, J., Alonso-Herrero, A., & Arag n-Salamanca, A. 2003, *MNRAS*, 338, 525
- P roux, C., Meiring, J. D., Kulkarni, V. P., Ferlet, R., Khare, P., Lauroesch, J. T., Vladilo, G., & York, D. G. 2006, *MNRAS*, 372, 369
- Petitjean, P., Ledoux, C., & Srianand, R. 2008, *A&A*, 480, 349
- Petitjean, P., Srianand, R., & Ledoux, C. 2000, *A&A*, 364, L26
- Pettini, M., Ellison, S. L., Bergeron, J., & Petitjean, P. 2002, *A&A*, 391, 21
- Pettini, M., Zych, B. J., Steidel, C. C., & Chaffee, F. H. 2008, *MNRAS*, 385, 2011
- Pilyugin, L. S. 1993, *A&A*, 277, 42
- Pilyugin, L. S. 2001, *A&A*, 374, 412
- Pilyugin, L. S., Vilchez, J. M., & Contini, T., 2004, *A&A*, 425, 849
- Prochaska, J. X., Chen, H., Wolfe, A. M., Dessauges-Zavadsky, M., & Bloom, J. S. 2008, *ApJ*, 672, 59
- Prochaska, J. X., Gawiser, E., Wolfe, A. M., Cooke, J., & Gelino, D. 2003, *ApJS*, 147, 227
- Prochaska, J. X., Henry, R. B. C., O’Meara, J. M., Tytler, D., Wolfe, A. M., Kirkman, D., Lubin, D., & Suzuki, N. 2002a, *PASP*, 114, 933
- Prochaska, J. X., Howk, J. C., O’Meara, J. M., Tytler, D., Wolfe, A. M., Kirkman, D., Lubin, D., & Suzuki, N. 2002b, *ApJ*, 571, 693
- Prochaska, J. X., Wolfe, A. M., Howk, J. C., Gawiser, E., Bures, S. M., & Cooke, J. 2007, *ApJS*, 171, 29
- Pustilnik, S. A., Pramskij, A. G., & Kniazev, A. Y. 2004, *A&A*, 425, 51
- Recchi, S., Matteucci, F. & D’Ercole, A., 2001, *MNRAS*, 322, 800
- Recchi, S., Matteucci, F. & D’Ercole, A., 2002, *A&A*, 384, 799
- Recchi, S., Matteucci, F., D’Ercole, A., & Tosi, M. 2004, *A&A*, 426, 37
- Recchi, S., Spitoni, E., Matteucci, F., & Lanfranchi, G. A. 2008, *A&A*, 489, 555
- Romano, D., Tosi, M., & Matteucci, F. 2006, *MNRAS*, 365, 759
- Rosenberg, J. L., Ashby, M. L. N., Salzer, J. J., & Huang, J.-S. 2006, *ApJ*, 636, 742
- Rupke D. S., Veilleux S., & Sanders D. B. 2005, *ApJS*, 160, 115
- Salpeter, E. E., 1955, *ApJ*, 121, 161
- Salzer, J. J., Lee, J. C., Melbourne, J., Hinz, J. L., Alonso-Herrero, A., & Jangren, A. 2005, *ApJ*, 624, 661
- Saviane, I., Ivanov, V. D., Held, E. V., Alloin, D., Rich, R. M., Bresolin, F., & Rizzi, L. 2008, *A&A*, 487, 901
- Scalo, J. M. 1986, *Fund. Cosmic Phys.*, 11, 1
- Schmidt, M. 1963, *ApJ*, 137, 758
- Schulte-Ladbeck, R. E., Hopp, U., Greggio, L., Crone, M. M., & Drozdovsky, I. O. 2001, *ApSSS*, 277, 309
- Searle, L. & Sargent, W. L. W. 1972, *ApJ*, 173, 25
- Searle, L., Sargent, W. L. W., & Bagnuolo, W. G. 1973, *ApJ*, 179, 427
- Skillman, E. D., Bomans, D. J., & Kobulnicky, H. A. 1997, *ApJ*, 474, 205
- Skillman, E. D., Kennicutt, R. C., & Hodge, P. W. 1989, *ApJ*, 347, 875
- Spergel, D. N., Bean, R., Dor e, O., Nolta, M. R., Bennett, C. L., Dunkley, J., Hinshaw, G., Jarosik, N., et al. 2007, *ApJS*, 170, 377
- Srianand, R. & Petitjean, P. 2001, *A&A*, 373, 816
- Srianand, R., Petitjean, P., Ledoux, C., Ferland, G., & Shaw, G. 2005, *MNRAS*, 362, 549
- Stasińska, G. & Izotov, Y. 2003, *A&A*, 397, 71
- Staveley-Smith, L., Davies, R. D., & Kinman, T. D. 1992, *MNRAS*, 258, 334
- Storrie-Lombardi, L. J. & Wolfe, A. M. 2000, *ApJ*, 543, 552
- Sullivan, M., Borgne, D. Le, Pritchett, C. J., Hodsmann, A., Neill, J. D., Howell, D. A., Carlberg, R. G., Astier, P., et al. 2006, *ApJ*, 648, 868
- Thuan, T. X. 2008, *IAUS*, 255, 348
- Thuan, T. X., Izotov, Y. I., & Foltz, C. B. 1999, *ApJ*, 525, 105
- Thuan, T. X., Izotov, Y. I., & Lipovetsky, V. A. 1995, *ApJ*, 445, 108
- Tosi, M., Greggio, L., Marconi, G., & Focardi, P. 1991, *AJ*, 102, 951
- Tremonti, C. A., Heckman, T. M., Kauffmann, G., Brinchmann, J., Charlot, S., White, S. D. M., Seibert, M., Peng, E. W., et al. 2004, *ApJ*, 613, 898
- Vaduvescu, O., McCall, M. L., & Richer, M. G., 2007, *AJ*, 134, 604
- Vaduvescu, O., McCall, M. L., Richer, M. G., & Fingerhut, R. L. 2005, *AJ*, 130, 1593
- Vaduvescu, O., Richer, M. G., & McCall, M. L. 2006, *AJ*, 131, 1318
- van den Hoek, L. B., & Groenewegen, M. A. T. 1997, *A&AS*, 123, 305
- van Zee, L. & Haynes, M. 2006, *ApJ*, 636, 214
- van Zee, L., Haynes, M. P., & Salzer, J. J. 1997, *AJ*, 114, 2497
- van Zee, L., Skillman, E. D., & Salzer, J. J. 1998, *AJ*, 116, 1186
- V zquez, G. A., Carigi, L., & Gonz lez, J. J. 2003, *A&A*, 400, 31
- Vladilo, G. 2004, *A&A*, 421, 479
- White, S. D. M. & Frenk C. S. 1991, *ApJ*, 379, 52
- Woosley, S. E. & Weaver, T. A., 1995, *ApJS*, 101, 181
- Zaritsky, D., Kennicutt, R. C., Jr., & Huchra, J. P. 1994, *ApJ*, 420, 87